METTL3 regulates viral m6A RNA modification and host cell innate immune responses during SARS-CoV-2 infection

Graphical abstract
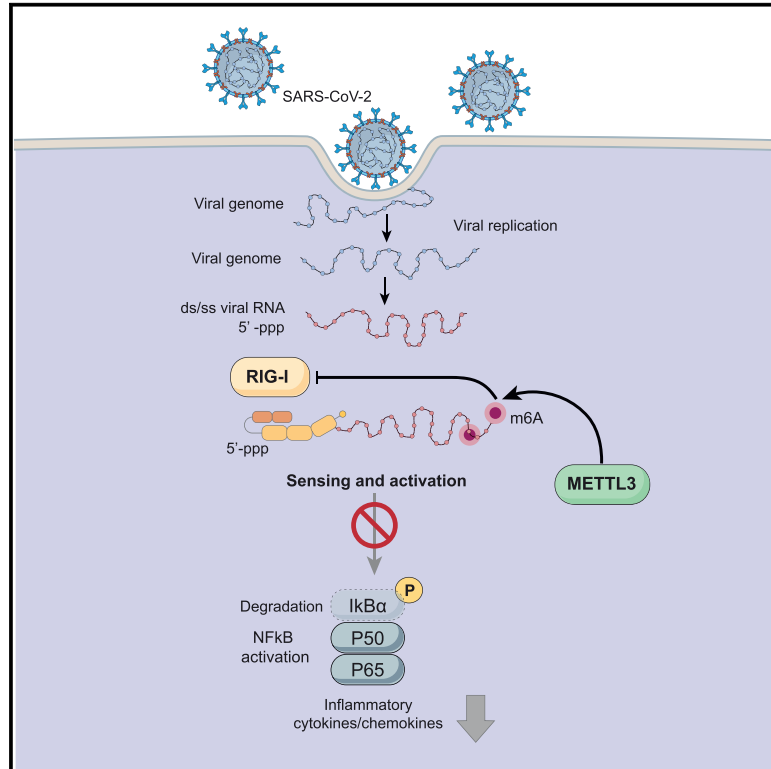
Authors

Na Li, Hui Hui, Bill Bray, ...,
Yinsheng Wang, Aaron F. Carlin,
Tariq M. Rana

Correspondence

trana@ucsd.edu

In brief

Li et al. show that SARS-CoV-2 RNA contains N^6-methylation of adenosine (m6A) modifications enriched at the 3′ end that play roles in evading host immune responses to viral infection. Host cell m6A methyltransferase METTL3 adds m6A modifications in SARS-CoV-2 RNA, leading to decreased RIG-I binding and subsequently dampening the sensing and activation of innate immune responses.

Highlights

- SARS-CoV-2 virus genome contains m6A modifications enriched in the 3′ end region of RNA

- RIG-I binds to SARS-CoV-2 viral RNAs, which is inhibited by m6A RNA modifications

- METLL3 regulates SARS-CoV-2 RNA m6A levels and activation of inflammation pathways

- METTL3 is reduced and inflammatory genes are induced in severe COVID-19 patients

CellPress

Cell Reports

Article

METTL3 regulates viral m6A RNA modification and host cell innate immune responses during SARS-CoV-2 infection

Na Li,[1,2] Hui Hui,[1,2,3] Bill Bray,[1,2] Gwendolyn Michelle Gonzalez,[7] Mark Zeller,[8] Kristian G. Anderson,[8] Rob Knight,[2,4,5] Davey Smith,[6] Yinsheng Wang,[7] Aaron F. Carlin,[6] and Tariq M. Rana[1,2,9,*]

[1]Division of Genetics, Program in Immunology, Institute for Genomic Medicine, University of California, San Diego, 9500 Gilman Drive MC 0762, La Jolla, CA 92093, USA
[2]Department of Pediatrics, University of California, San Diego, 9500 Gilman Drive MC 0762, La Jolla, CA 92093, USA
[3]Bioinformatics Program, University of California, San Diego, 9500 Gilman Drive, La Jolla, CA 92093, USA
[4]Department of Bioengineering, University of California, San Diego, 9500 Gilman Drive, La Jolla, CA 92093, USA
[5]Center for Microbiome Innovations, University of California, San Diego, 9500 Gilman Drive, La Jolla, CA 92093, USA
[6]Division of Infectious Diseases and Global Public Health, Department of Medicine, University of California, San Diego, 9500 Gilman Drive, La Jolla, CA 92093, USA
[7]Environmental Toxicology Graduate Program and Department of Chemistry, University of California, Riverside, Riverside, CA 92521, USA
[8]Department of Immunology and Microbiology, Scripps Research, 10550 North Torrey Pines Road, La Jolla, CA 92037, USA
[9]Lead contact
*Correspondence: trana@ucsd.edu
https://doi.org/10.1016/j.celrep.2021.109091

SUMMARY

It is urgent and important to understand the relationship of the widespread severe acute respiratory syndrome coronavirus clade 2 (SARS-CoV-2) with host immune response and study the underlining molecular mechanism. N^6-methylation of adenosine (m6A) in RNA regulates many physiological and disease processes. Here, we investigate m6A modification of the SARS-CoV-2 gene in regulating the host cell innate immune response. Our data show that the SARS-CoV-2 virus has m6A modifications that are enriched in the 3′ end of the viral genome. We find that depletion of the host cell m6A methyltransferase METTL3 decreases m6A levels in SARS-CoV-2 and host genes, and m6A reduction in viral RNA increases RIG-I binding and subsequently enhances the downstream innate immune signaling pathway and inflammatory gene expression. METTL3 expression is reduced and inflammatory genes are induced in patients with severe coronavirus disease 2019 (COVID-19). These findings will aid in the understanding of COVID-19 pathogenesis and the design of future studies regulating innate immunity for COVID-19 treatment.

INTRODUCTION

Coronavirus disease 2019 (COVID-19) caused by severe acute respiratory syndrome coronavirus clade 2 (SARS-CoV-2) has become a globe health emergency since its outbreak in 2019 (Lu et al., 2020b). Aged and immune-deficient people are more prone to complications and death by infection. The immune response to the viral infection is an important step to control viral replication and pathological symptoms such as acute respiratory distress syndrome (ARDS) (Huang et al., 2020; Xu et al., 2020). Innate immune signaling is the first response of the host cell to viral infection. Pattern recognition receptors (PRRs) such as RIG-I-like receptor (RLR) and Toll-like receptor (TLR) recognize pathogen-associated molecular patterns (PAMPs) of virus and activate signaling cascades to stimulate interferon (IFN) and inflammatory cytokines and chemokines to mount the initial antiviral response (Jensen and Thomsen, 2012). The induced cytokines and chemokines are required for initial immune response but excessive activation may cause cytokine storm and ARDS

and exacerbate the disease at late stage (Catanzaro et al., 2020; Qin et al., 2020; Xu et al., 2020). SARS-CoV-2 has evolved mechanisms to escape the host cell innate immune response, such as mimicking the host capping machinery and 2′-O-methylation by its Nsp16/Nsp10 complex in ORF1ab or inhibiting IFN production and downstream IFN signaling by Nsp1/Nsp3/ Nsp6/Nsp12/Nsp13/Nsp14/Nsp15, ORF3a/ORF6/ORF7, or membrane (M) (Krafcikova et al., 2020; Lei et al., 2020; Xia et al., 2020; Yuen et al., 2020).Viruses may also utilize host cell components to evade immune surveillance. Studies have shown that RNA modifications such as N^6-methylation of adenosine (m6A) greatly suppress innate immune recognition and RIG-I binding or innate immune response (Durbin et al., 2016; Karikó et al., 2005; Kim et al., 2020; Lu et al., 2020a). m6A is the most abundant and widely studied internal RNA modification in eukaryotes, and it has been found in several types of viruses, including the ones that only replicate in cytoplasm, such as Hepatitis C virus (HCV), Zika Virus (ZIKV), Dengue virus (DENV), West Nile Virus (WNV), and yellow fever virus (Gokhale et al., 2016;
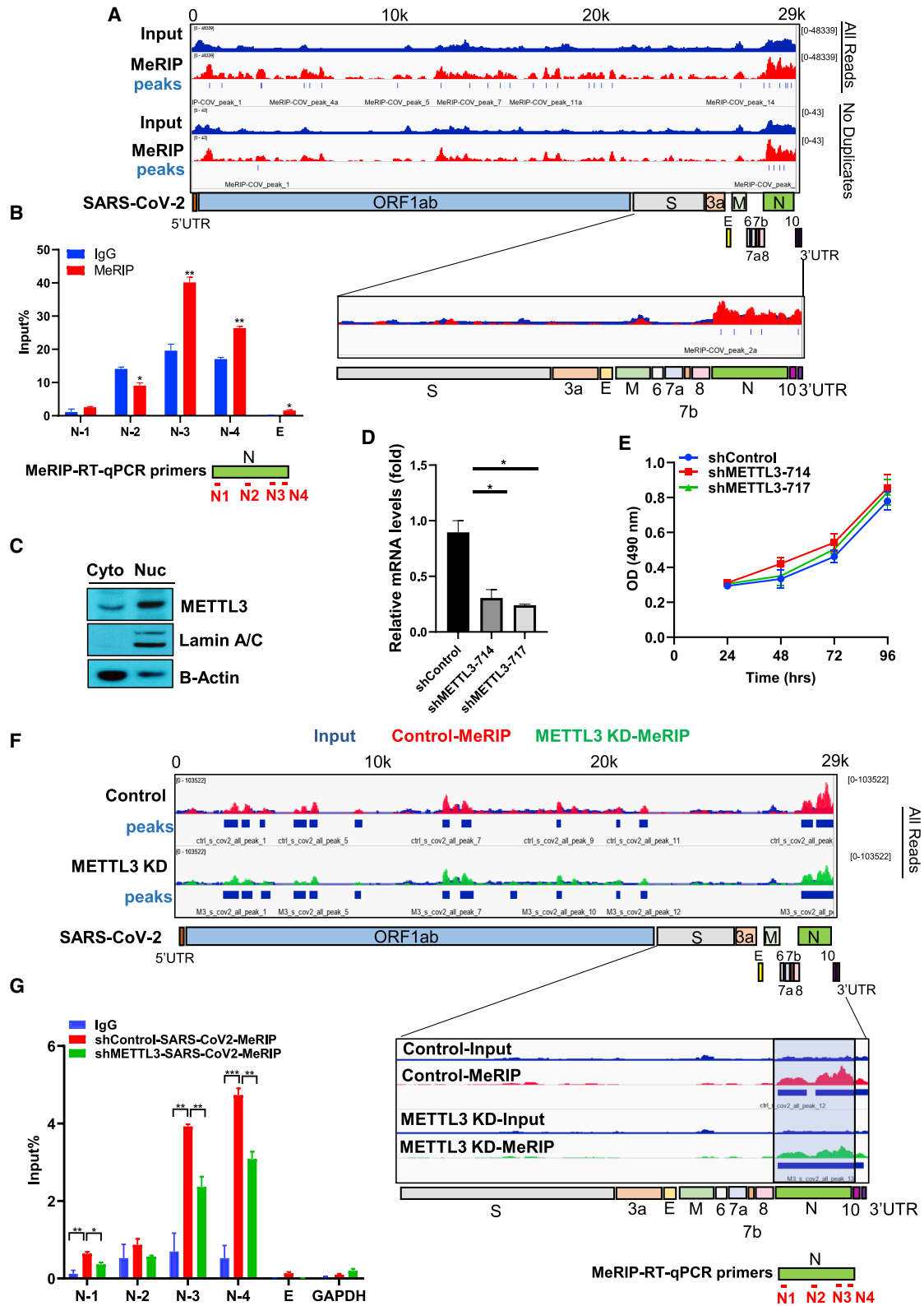
Hao et al., 2019; Lichinchi et al., 2016b; McIntyre et al., 2018). m6A plays important roles in viral replication, RNA assembly, and innate immune responses (Gokhale et al., 2016; Lichinchi et al., 2016b; Lu et al., 2020a). It is urgent and important to determine whether the SARS-CoV-2 genome contains RNA modifications and their functional relevance to the host cell innate immune response during viral infection. In this study, we report the presence of m6A modification in SARS-CoV-2 RNA and discover the roles and molecular mechanism of m6A of the viral genome and host factors in the host cell innate response during SARS-CoV-2 infection.

RESULTS

SARS-CoV-2 viral RNA is chemically modified, and m6A is enriched in the nucleocapsid (N) region of the viral genome

To investigate the epitranscriptomic profile of the SARS-CoV-2 virus, we purified viral RNA from Vero cells, analyzed its purity, and examined RNA chemical modifications by mass spectrometry (Figures S1A and S1B). By using liquid chromatography-tandem mass spectrometry (LC-MS/MS and MS/MS/MS), together with stable-isotope-labeled ribonucleosides as internal standards or surrogate standards, we were able to reliably detect a number of modified ribonucleosides in SARS-CoV-2 RNA, including 2′-O-methylated derivatives of all four canonical nucleosides (Am, Cm, Um, and Gm), several modified cytidine derivatives (ac^4C, m^3C, and m^5C), two modified uridine derivatives (Ψ and m5U), and two modified adenosines (m6A and m6,6A). Additionally, we were also able to detect 2-thiocytidine, though its level was not quantified. Among these modifications, m6A accounts for 0.096% of adenosine in the virus, and the estimated number of m6A-modified sites is 8 (8,954 adenosines × 0.096%) (Figure S1B).

To validate the mass spectrometric data and examine the distribution of m6A, we performed methylated (m6A) RNA immunoprecipitation sequencing (MeRIP-seq) for the full-length SARS-CoV-2 viral RNA purified from Vero cells. In order to obtain the most reliable regions and peaks of m6A in the genome, we

applied two different aligners (STAR and Bowtie2) and peak calling methods (MACS2 and m6A viewer), as well as removed or did not remove duplicates, to further confirm the common regions and peaks of m6A in the SARS-CoV-2 genome. We found that m6A peaks are present in ORF1ab and 3′ end of viral genome, especially the N region of SARS-CoV-2 viral RNA detected by every method and strategy we used (Figures 1A and S1C–S1E). We have summarized the detected peak regions in Table S1. To further validate our MeRIP-seq data, we performed MeRIP-qRT-PCR for SARS-CoV-2 viral RNA purified from Vero cells to assess m6A enrichment over immunoglobulin G (IgG) control by using four different primers in the N region and one primer in the envelope (E) region. As shown in Figure 1B, we observed m6A modification enriched in N-3 and N-4 regions, while other regions had limited enrichment over IgG (N-1 and N-2) or very few immunoprecipitation (IP) fragments (E). Altogether, these results show that SARS-CoV-2 viral RNA contains m6A modifications, which are enriched in the N region of the viral genome.

METTL3 knockdown (KD) reduces m6A modification of SARS-CoV-2 RNA

To determine whether the m6A modification in SARS-CoV-2 RNA was regulated by the host RNA methyltransferase complex, we depleted METTL3, which is a catalytic subunit of m6A methyltransferase complex, and analyzed m6A levels in viral RNA. First, we examined METTL3 subcellular localization, and it was readily detected in both the cytosolic (Cyto) and nuclear (Nuc) fractions of SARS-CoV-2-permissive human colorectal adenocarcinoma Caco-2 cells (Figure 1C). Then, we knocked down METTL3 using two different small hairpin RNAs (shRNAs) in Caco-2 cells, and cell viability and proliferation were not obviously affected by METTL3 depletion (Figures 1D and 1E). Caco-2 stable cell lines expressing shRNAs for non-targeting control or METTL3 were infected with USA-WA1/2020 SARS-CoV-2 at MOI = 2 and supernatant or cellular RNAs were extracted 24 h post-infection. Then, we performed MeRIP-seq for viral RNAs collected from infected Caco-2 cells, and then compared m6A levels of SARS-CoV-2 virus from control and

Figure 1. SARS-CoV-2 viral RNA contains m6A modifications, and METTL3 depletion reduced m6A levels in SARS-CoV-2 viral RNA

(A) Genome browser tracks for input and MeRIP of SARS-CoV-2 viral RNA isolated from Vero cells. Reads were aligned with Bowtie2, and peaks were called by MACS2 without removing duplicates (upper panel) or with removing duplicates (lower panel). Input is indicated in blue and MeRIP in red. Bed files of the called peaks are shown under the MeRIP track of each condition. The scale of the peak density is set to be the same for all groups and is shown in the corner. Enlarged view shows the enrichment of m6A signals in the nucleocapsid (N) region of the SARS-CoV-2 virus.

(B) MeRIP-qPCR of SARS-CoV-2 viral RNA. IgG control and m6A antibody were added in IP lysates containing equal amounts of viral RNA. Primers amplifying different regions of the N (N-1 to N-4) and E genes were used to quantify viral RNA. N = 2.

(C) METTL3 is present in both the nuclear and cytosolic fractions of Caco-2 cells. Levels of METTL3, the nuclear fraction marker lamin A/C, and the cytosolic fraction marker protein beta-actin were examined by western blotting.
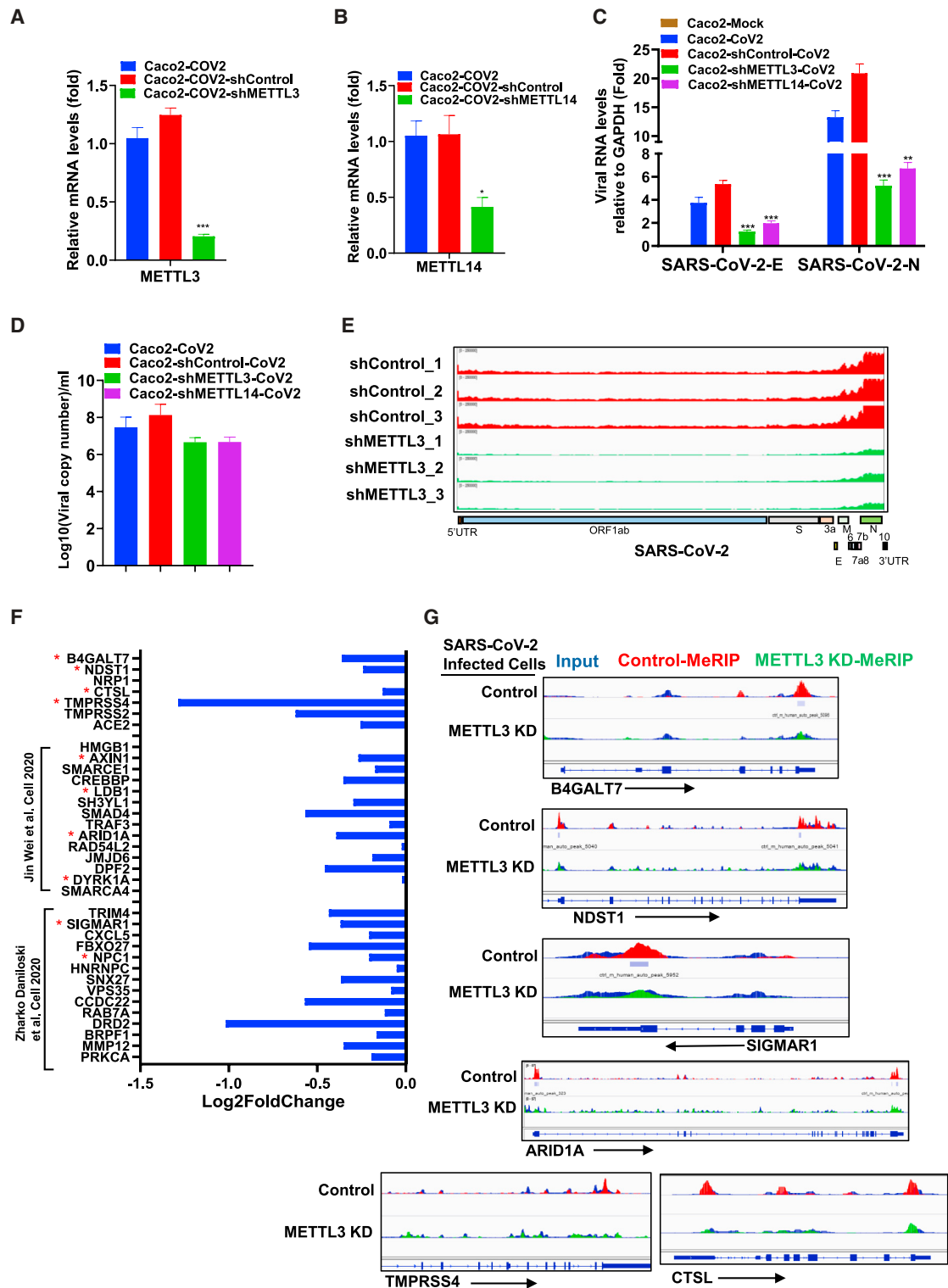
(D) METTL3 knockdown (KD) efficiency was examined by qRT-PCR in Caco-2 cells. Two different shRNAs were used to target METTL3. N = 3. Data are presented as the mean ± SEM. Group means were compared by Student's t test. *p < 0.05.

(E) Cell proliferation of control and METTL3 KD Caco-2 cells was evaluated by colorimetric MTS assay. N = 3.

(F) Genome browser tracks for input and MeRIP of SARS-CoV-2 viral RNA from control and METTL3 KD Caco-2 cells infected with SARS-CoV-2. Reads were aligned with STAR, and peaks were called by MACS2 without removing duplicates. Input is indicated in blue, MeRIP of control in red, and MeRIP of METTL3 KD in green. Bed files of the called peaks are shown under the MeRIP track of each condition. The scale of the peak density is set to be the same for all groups and is shown in the corner. Enlarged view shows the m6A signals in the N region of the SARS-CoV-2 virus.

(G) MeRIP-qPCR of viral RNAs from SARS-CoV-2-infected control and METTL3 KD Caco-2 cells. IgG control and m6A antibody were added in IP lysates containing equal amounts of viral RNA. Primers amplifying different regions of the N (N-1 to N-4) and E genes were used to quantify viral RNA. GAPDH served as a negative control. N = 3. Data are presented as the mean ± SEM. Group means were compared by Student's t test. *p < 0.05, **p < 0.01, and ***p < 0.001.

See also Figures S1 and S2 and Tables S1, S2, and S4.

A

Relative mRNA levels (fold)

- Caco2-COV2
- Caco2-COV2-shControl
- Caco2-COV2-shMETTL3

METTL3

***

B

Relative mRNA levels (fold)

- Caco2-COV2
- Caco2-COV2-shControl
- Caco2-COV2-shMETTL14

METTL14

*

C

Viral RNA levels relative to GAPDH (Fold)

- Caco2-Mock
- Caco2-CoV2
- Caco2-shControl-CoV2
- Caco2-shMETTL3-CoV2
- Caco2-shMETTL14-CoV2

SARS-CoV-2-E   SARS-CoV-2-N

*** ***   *** **

D

Log10(Viral copy number)/ml

- Caco2-CoV2
- Caco2-shControl-CoV2
- Caco2-shMETTL3-CoV2
- Caco2-shMETTL14-CoV2

E

shControl_1
shControl_2
shControl_3
shMETTL3_1
shMETTL3_2
shMETTL3_3

5'UTR   ORF1ab   S   3a M   N
SARS-CoV-2   6 7b 10
E 7a8 3'UTR

F

* B4GALT7
* NDST1
NRP1
* CTSL
* TMPRSS4
TMPRSS2
ACE2
HMGB1
* AXIN1
SMARCE1
CREBBP
* LDB1
SH3YL1
SMAD4
TRAF3
* ARID1A
RAD54L2
JMJD6
DPF2
* DYRK1A
SMARCA4

(Jin Wei et al, Cell 2020)

TRIM4
* SIGMAR1
CXCL5
FBXO27
* NPC1
HNRNPC
SNX27
VPS35
CCDC22
RAB7A
DRD2
BRPF1
MMP12
PRKCA

(Zharko Daniloski et al, Cell 2020)

-1.5   -1.0   -0.5   0.0
Log2FoldChange

G

SARS-CoV-2 Infected Cells   Input   Control-MeRIP   METTL3 KD-MeRIP

Control
METTL3 KD
B4GALT7

Control
METTL3 KD
NDST1

Control
METTL3 KD
SIGMAR1

Control
METTL3 KD
ARID1A

Control
METTL3 KD
TMPRSS4

CTSL

Figure 2. METTL3 depletion reduced viral load and proviral gene expression during SARS-CoV-2 infection

(A and B) METTL3 (A) and METTL14 (B) KD efficiency was examined by qRT-PCR in Caco-2, Caco-2-shControl, Caco-2-shMETTL3 (A), or Caco-2-shMETTL14 (B) cells after SARS-CoV-2 infection. N = 3. Data are presented as the mean ± SEM. Group means were compared by Student's t test. $p < 0.05$ and $p < 0.001$.

(legend continued on next page)

METTL3 depleted cells (Lichinchi et al., 2016a, 2016b; Lichinchi and Rana, 2019). As shown in Figure 1F, m6A peaks were detected in ORF1ab and the 3′ end of the viral genome, especially the N region of viral RNAs from infected Caco-2 cells, which is similar to the detected m6A peaks in virus obtained from Vero cells (Figure 1A; Table S2). More importantly, we observed a decreased m6A occupancy in the N region of SARS-CoV-2 virus from METTL3-depleted cells compared to control (Figure 1F; Table S2). We further validated the MeRIP-seq data by MeRIP-RT-qPCR as shown in Figure 1G (Li et al., 2020; Wang et al., 2020a). Similar to SARS-CoV-2 viral RNA isolated from Vero cells, we observed that N-3 and N-4 regions are the most enriched m6A regions in N compared to IgG control. METTL3 depletion significantly reduced m6A levels in those regions compared to control (Figure 1G).

Next, we performed MeRIP-seq for cellular RNAs from SARS-CoV-2-infected control and METTL3 KD Caco-2 cells. Consistently, the results also showed a reduction in m6A signals in the N region of the virus with or without removing the duplicate reads in METTL3-depleted cells compared to control (Figure S2A; Table S2). Altogether, these data showed that METTL3 depletion in human Caco-2 cells reduced SARS-CoV-2 m6A levels, with the most obvious reduction of m6A in the 3′ viral genomic region by METTL3 depletion.

Depletion of m6A methyltransferase METTL3 decreases SARS-CoV-2 viral load and reduces proviral gene expression in host cells

Next, we sought to determine the function of METTL3 and m6A modification during SARS-CoV-2 viral infection. We prepared Caco-2 cells stably expressing shRNAs with non-targeting control sequences or targeting m6A methyltransferase METTL3 or METTL14. Cells were infected with USA-WA1/2020 SARS-CoV-2 at MOI = 2, and RNA from cellular and supernatant fractions was isolated 24 h post-infection as described previously (Tiwari et al., 2021; Wang et al., 2020b). Depletion of METTL3 and METTL14 was confirmed before infection (Figures S2B and S2C) and after SARS-CoV-2 infection by RT-qPCR (Figures 2A-B). The presence of SARS-CoV-2 viral genome was confirmed in supernatant or cellular RNA after viral infection (Figures 2C, 2D, and S2D). Our quantitative analysis of viral genes in supernatant or cellular RNA after infection showed that the viral load was reduced in METTL3- or METTL14-depleted Caco-2 cells during SARS-CoV-2 infection (Figure 2C). We next performed RNA sequencing (RNA-seq) for cellular RNAs from

shControl and shMETTL3 Caco-2 cells after SARS-CoV-2 infection. Viral RNA analysis from RNA-seq further confirmed that the viral gene content was greatly reduced in METTL3-depleted cells after viral infection (Figure 2E). These results suggested that suppressing m6A by depletion of methyltransferases METTL3/14 reduced the SARS-CoV-2 viral load in infected cells.

We analyzed host gene expression affected by METTL3 KD in Caco2 cells during SARS-CoV-2 infection. As several host proviral genes have recently been identified or validated to be essential for the SARS-CoV-2 life cycle (Cantuti-Castelvetri et al., 2020; Clausen et al., 2020; Daniloski et al., 2021; Hoffmann et al., 2020; Wei et al., 2021; Zang et al., 2020; Zhou et al., 2020), we examined the expression of these proviral genes in control and METTL3 KD cells during SARS-CoV-2 infection. As shown in Figure 2F, RNA expression of several of the proviral genes was decreased in METTL3 KD cells compared to the control-shRNA-treated cells. To determine the m6A signals of the downregulated proviral genes in control and METTL3 KD cells, MeRIP-seq was performed for cellular RNAs upon SARS-CoV-2 infection. We found that m6A signals were also decreased in some of the SARS-CoV-2 proviral host factors in METTL3 KD cells during SARS-CoV-2 infection (Figures 2G, S2E, and S2F; Table S2). Altogether, our findings of reduced viral load and proviral host factors expression and decreased m6A levels of those genes in METTL3-depleted Caco-2 cells suggested a vital role of METTL3 in regulating m6A levels and the host response to SARS-CoV-2 infection.

Depletion of m6A methyltransferase METTL3 enhances the expression of host cell innate immune signaling effector molecules during SARS-CoV-2 infection

m6A modification is an important mechanism for exogenous RNAs to evade the host innate immune response (Durbin et al., 2016; Karikó et al., 2005; Kim et al., 2020; Lu et al., 2020a). To investigate the role of m6A modification of SARS-CoV-2 viral RNA in the host cell innate immune response, we asked whether modulating m6A abundance by depletion of host m6A methyltransferases would alter host innate immune signaling effector gene expression during SARS-CoV-2 infection. SARS-CoV-2 viral replication and innate immune responses to viral infection in human colorectal carcinoma Caco-2 cells resemble *ex-vivo*-cultured normal human bronchus, lung, and alveolar epithelial cells (Hui et al., 2020). Therefore, we performed the following experiments in Caco-2 cells. RNA-seq was performed for control and METTL3 KD Caco-2 cells upon SARS-CoV-2 infection.


(C) SARS-CoV-2 gene expression of mock-infected Caco-2 cells, and SARS-CoV-2-infected Caco-2, Caco-2-shControl, Caco-2-shMETTL3, and Caco-2-shMETTL14 cells. Cells were collected for RNA extraction and RT-qPCR analysis. Fold change of SARS-CoV-2 N and E genes over GAPDH were calculated and are presented. N = 3. Data are presented as the mean ± SEM. Group means were compared by Student's t test. **p < 0.01, ***p < 0.001.

(D) SARS-CoV-2 viral genome copy number of infected Caco-2, Caco-2-shControl, Caco-2-shMETTL3, and Caco-2-shMETTL14 cells. Supernatants were collected for RNA extraction and qRT-PCR detection. N = 3.

(E) Read coverage of SARS-CoV-2 genome of viral infected shControl and shMETTL3 Caco-2 cells analyzed by RNA-seq. The scale of all the samples was set to be the same. N = 3.

(F) Downregulated proviral host genes in METTL3-depleted Caco-2 cells compared with control cells during SARS-CoV-2 infection. The red star marks genes with altered m6A levels determined by MeRIP-seq for cellular RNAs in control and METTL3 KD cells during SARS-CoV-2 infection.

(G) Genome browser tracks for examples of the downregulated proviral genes with reduced m6A levels (listed in F and marked with a red star) in METTL3 KD cells compared with control Caco-2 cells during SARS-CoV-2 infection. Input is indicated in blue, MeRIP of control in red, and MeRIP of METTL3 KD in green. Bed files of the called peaks are shown under the MeRIP track of each condition. The scale of the peak density is set to be the same in the control and METTL3 KD groups.
See also Figure S2 and Tables S2, S3, and S4.
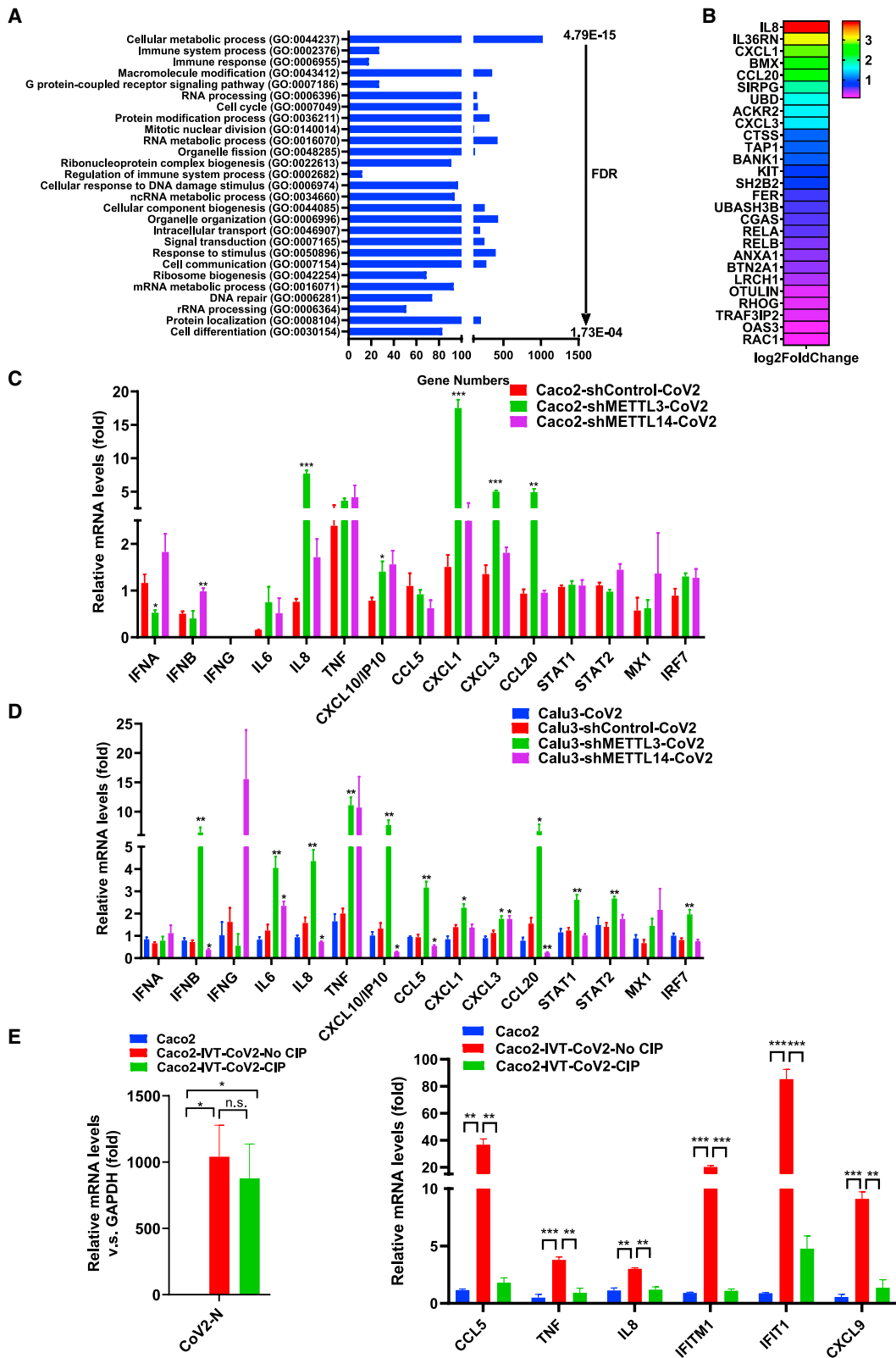
A
(legend on next page)

Gene Ontology (GO) analysis of the differentially expressed genes (DEGs) showed that METTL3-KD-regulated genes were involved in diverse cellular processes, including metabolic processes, immune response, RNA processing, cell cycle, biogenesis, signaling pathways, ribosome function, protein modification and location, DNA repair, and cell differentiation (Figures 3A and S2G). Notably, immune response genes were enriched in METTL3-depleted cells after viral infection, which indicates an early response of the host cell to viral infection and may directly link to the altered viral m6A modification levels (Figures 3A and 3B). In METTL3-depleted cells, after viral infection, RNA-seq showed that the upregulated immune response genes included inflammatory cytokines and chemokines, including interleukin-8 (IL-8), CXCL1, CXCL3, and CCL20, among others (Figure 3B). We did not observe significantly altered IFN genes expression or m6A levels in METTL3 KD cells, suggesting that the upregulation of cytokines/chemokines was not dependent on IFN genes in METTL3 KD Caco-2 cells upon SARS-CoV-2 infection (Tables S2 and S3). Furthermore, we examined effector genes of innate immune response for their mRNA expression in control or METTL3- or METTL14-depleted Caco-2 cells upon SARS-CoV-2 infection by qRT-PCR. The primers used are summarized in Table S4. The genes include type I and II IFNs (IFNα, IFNβ1, and IFNγ), inflammatory cytokines (IL-6, IL-8, and tumor necrosis factor [TNF]), chemokines (CXCL10/IP10, CCL5, CXCL1, CXCL3, and CCL20), and IFN-stimulated genes (ISGs) (STAT1, STAT2, MX1, and IRF7). We confirmed that both METTL3 and METTL14 depletion increased cytokine and chemokine expression (IL-6, IL-8, TNF, CXCL10/IP10, CXCL1, and CXCL3), and METTL3 depletion has more dramatic and significant effects; however, IFN genes and ISGs were slightly induced or not changed in METTL3-depleted cells compared to control during SARS-CoV-2 viral infection (Figure 3C). In addition, the expression of these inflammation genes was not significantly changed in METTL3-depleted cells without viral infection (Figure S3A). These data suggest that the upregulation of chemokine/cytokine gene expression in METTL3-depleted cells is dependent on viral infection.

To validate our findings, we used lung epithelial cells (Calu-3) to perform a similar experiment. Calu-3 cells were reported to induce IFN expression after SARS-CoV-2 infection compared with noninfected cells under the same infection conditions we used (MOI = 2; cells were collected at 24 h post-infection) (Blanco-Melo et al., 2020). First, we checked type I IFN expres-sion before and after viral infection, and we found that IFNα and IFNβ expression was increased after viral infection, with over 10-fold induction for IFNβ after infection compared with noninfected cells (Figure S3B). In addition, IFNβ is the most abundant gene among type I and II IFNs after SARS-CoV-2 infection (Figure S3C). Next, we examined gene KD efficiency of METTL3 and METTL14 after viral infection by qRT-PCR (Figures S3D and S3E). SARS-CoV-2 infection was confirmed by examining viral genes after infection (Figure S3F). Notably, unlike in Caco-2 cells, METTL3 KD in Calu-3 cells decreased cell proliferation without viral infection. We then examined downstream innate immune effector gene expression in Calu-3 cells during SARS-CoV-2 infection. We found that compared with control cells, METTL3 depletion significantly enhances IFNβ and ISG expression (STAT1, STAT2, and IRF7) and cytokine/chemokine expression (IL-6, IL-8, TNF, CXCL10/IP10, CCL5, CXCL1, CXCL3, and CCL20) after SARS-CoV-2 infection, while METTL14 KD only increased IFNγ, IL-6, TNF, and CXCL3 levels (Figure 3D). In summary, we found that METTL3 has more dramatic and significant effects on upregulation of inflammatory gene expression than METTL14 depletion in both Caco-2 and Calu-3 cells during SARS-CoV-2 infection. The effects of METTL3 depletion on increased inflammatory cytokine/chemokine expression are not dependent on IFN gene induction and only occur during SARS-CoV-2 infection.

RIG-I binds to SARS-CoV-2 RNA to stimulate inflammatory gene expression

Our results thus far showed that the SARS-CoV-2 genome has m6A modifications that are enriched in the N region and that depletion of the host cell m6A methyltransferase METTL3 enhances innate immune signaling target inflammatory gene expression during SARS-CoV-2 infection. Next, we strived to delineate the mechanisms of m6A modification of the SARS-CoV-2 gene in regulating the innate immune response. Recognizing PAMPs by host cell PRRs is the upstream event of inflammatory gene induction during RNA viral infection (Akira et al., 2006). There are two major PRRs in early innate immune responses to viral infections, TLRs and RLRs (Brubaker et al., 2015; Loo and Gale, 2011). Unlike TLR, which are mainly expressed in dendritic cells (DCs) or macrophages, RLRs are reported to be widely expressed cytoplasmic sensors of double-stranded/single stranded (ds/ss) viral RNA (Jensen and Thomsen, 2012; Totura and Baric, 2012). Similarly, we found that

Figure 3. METTL3/METTL14 depletion enhances innate immune response effector gene expression during SARS-CoV-2 infection

(A) Gene Ontology (GO) analysis of upregulated genes comparing shMETTL3 with shControl Caco-2 cells after SARS-CoV-2 infection. All of the biological process categories shown have a false discovery rate (FDR) < 0.001.

(B) Log2 fold change of shMETTL3 compared with shControl Caco-2 cells is shown for upregulated immune response genes after SARS-CoV-2 infection.

(C) Gene expression of innate immune pathway downstream effectors was examined in shControl, shMETTL3, or shMETTL14 Caco-2 cells after SARS-CoV-2 infection. Gene expression changes were compared between shControl and KD cells. N = 3. Data are presented as the mean ± SEM. Group means were compared by Student's t test. *p < 0.05, **p < 0.01, and ***p < 0.001.

(D) Gene expression of innate immune pathway downstream effectors was examined in Calu-3, shControl, shMETTL3, or shMETTL14 Calu-3 cells after SARS-CoV-2 infection. Gene expression changes were compared between shControl and KD cells. N = 3. Data are presented as the mean ± SEM. Group means were compared by Student's t test. *p < 0.05, **p < 0.01, and ***p < 0.001.

(E) 1.2 × 10^13 copies of IVT-SARS-CoV-2-N (IVT-CoV-2) RNA with or without calf alkaline phosphatase (CIP) were transfected to Caco-2 cells seeded in 24-well plates, and downstream inflammatory and ISG gene expression was examined by qRT-PCR. N = 3. Data are presented as the mean ± SEM. Group means were compared by Student's t test. *p < 0.05, **p < 0.01, and ***p < 0.001.

See also Figures S2 and S3 and Tables S3 and S4.
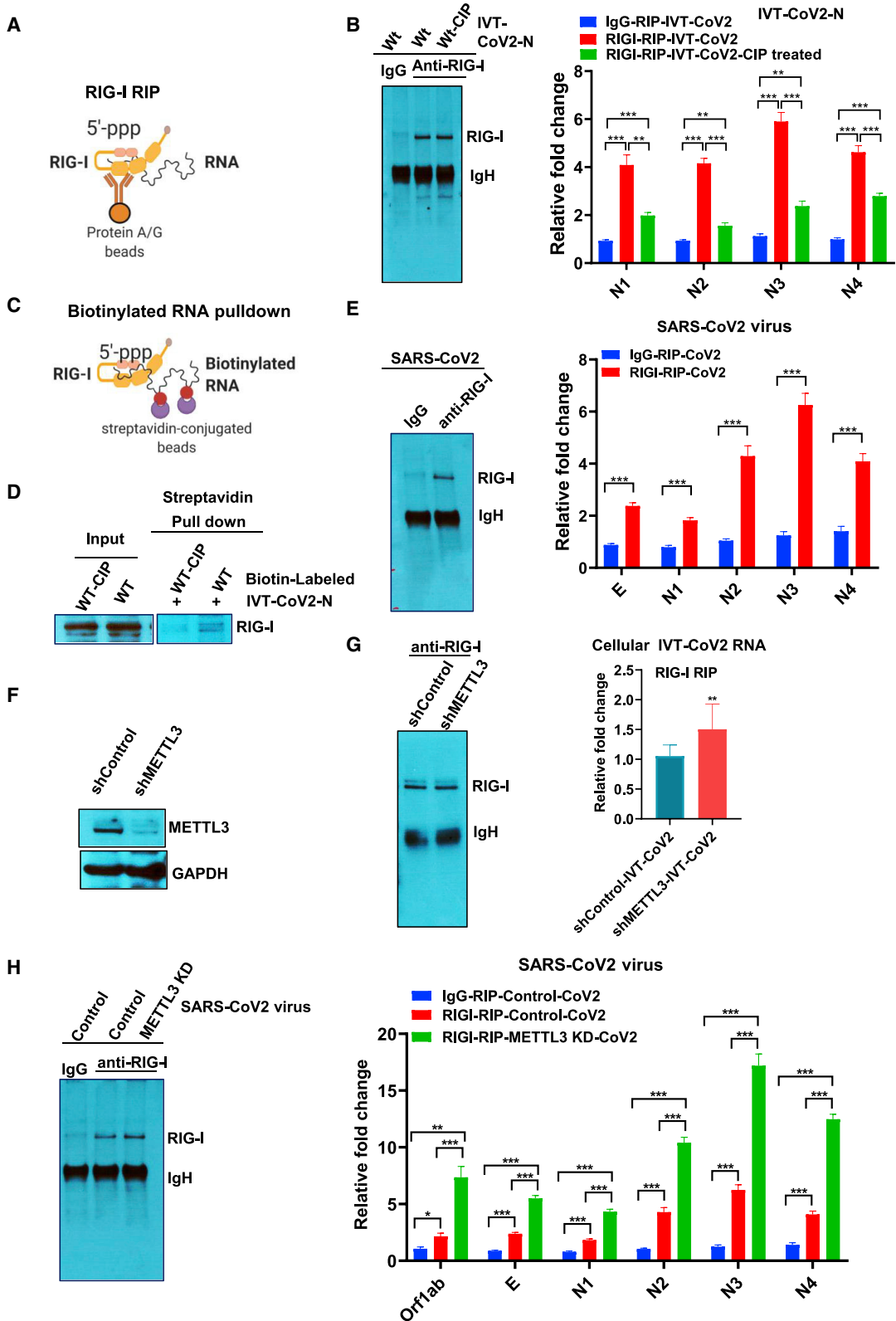
(legend on next page)

RIG-I is the most expressed upstream RLR/TLR in Caco2 cells during SARS-CoV-2 infection, and there was no significant change in RIG-I expression in METTL3 KD cells during SARS-CoV-2 infection (Table S3). In addition, m6A levels in RIG-I or any of the innate immune signaling pathway genes were not changed (Table S2). RLRs were reported to recognize a murine coronavirus to induce innate immune response (Li et al., 2010), and it was reported that m6A modification of viral RNA diminishes the innate immune response by reduced RIG-I binding (Durbin et al., 2016; Karikó et al., 2005). Therefore, we reasoned that the upregulation of inflammation genes in METTL3-depleted cells during SARS-CoV-2 infection may be due to the altered immune signaling mediated by recognition of RIG-I with modified viral RNA.

To test our hypothesis and investigate the mechanisms, we prepared *in-vitro*-transcribed (IVT) capped and uncapped N region of SARS-CoV-2 virus, which showed enriched m6A modification by MeRIP-seq (Figure 1). We transfected the IVT RNA in three different cell lines to analyze the induction of innate immune downstream effectors. In all the three cell lines we tested, IVT SARS-CoV-2-N RNA successfully induced IFNβ and cytokine/chemokine expression (such as IL-6/IL-8, TNF, CXCL10/IP10, and CCL5) (Figures S3G–S3I). Among these cell lines, Caco-2 showed more dramatic reduction of inflammatory gene expression when transfecting capped comparing with uncapped RNA. As 5′-capped RNA does not trigger RIG-I recognition and downstream signaling activation (Kell and Gale, 2015), these results again indicate a potential role of RIG-I in inducing the innate immune response in Caco-2 cells (Figures S3G–S3I). Since METTL3 depletion did not cause cell death or alteration of cell survival in Caco-2 cells upon SARS-CoV-2 infection, we performed the following experiments using uncapped IVT SARS-CoV-2-N RNA (IVT CoV-2) in Caco-2 cells. First, we examined inflammatory gene and ISG expression by transfecting IVT CoV-2 RNAs that retained 5′ phosphorylated groups or were treated with calf intestinal phosphatase (CIP). We observed that the induction of inflammatory gene and ISG expression was substan-

tially reduced in CIP-treated IVT CoV-2 RNA compared to the nontreated group (Figure 3E). As 5′ phosphorylation is essential for RIG-I binding (Wang et al., 2010), our results suggested that RIG-I binding to SARS-CoV-2 RNA may be important for stimulation of downstream inflammatory gene expression during viral infection. To validate the role of RIG-I in mediating the METTL3-regulated innate immune response, we performed RIG-I RNA IP (RIP) experiments by immunoprecipitating RIG-I in cell lysates followed by detecting RIG-I-bound RNAs (Figure 4A). When incubated with similar amounts of RIG-I (Figure 4B, right panel immunoblot), IVT CoV-2 RNA binds to RIG-I, and CIP treatment of RNA greatly reduced RIG-I binding to IVT CoV-2 RNA (Figure 4B, right panel). To confirm these results, we also applied a biotinylated RNA pull-down assay to examine the binding of RIG-I to biotinylated IVT CoV-2 RNA. Similarly, we found that wild-type, but not CIP-treated, IVT CoV-2 RNAs bind to RIG-I (Figures 4C and 4D). Next, we performed RIG-I RIP using SARS-CoV-2 viral RNA from SARS-CoV-2-infected Caco-2 cells and found that RIG-I binds to SARS-CoV-2 RNA compared to IgG control, which is in line with the IVT CoV-2 results (Figure 4E). All in all, these data show that RIG-I binds to SARS-CoV-2 RNA, which is the upstream event of the inflammatory gene stimulation during SARS-CoV-2 infection.

Depletion of the m6A methyltransferase METTL3 enhances RIG-I binding to SARS-CoV-2 RNA

After determining the binding of RIG-I to SARS-CoV-2 RNA, we studied the role of m6A modification of SARS-CoV-2 RNA in RIG-I recognition. First, we tested whether depletion of the m6A methyltransferase METTL3 in host cells would change RIG-I binding to the transfected cellular IVT-CoV-2 RNA. METTL3 protein levels were greatly reduced in METTL3-depleted Caco-2 cells (Figure 4F), and m6A levels of transfected IVT CoV-2 RNA were also reduced in METTL3-depleted Caco-2 cells (Figure S3J). In RIP experiments, RIG-I proteins were precipitated at similar levels in control and METTL3 KD cells (Figure 4G, left panel), and RIG-I-bound transfected cellular

Figure 4. Reduction of m6A levels in SARS-CoV-2 viral RNA by METTL3 depletion leads to an increased recognition by RIG-I

(A) Graphic illustration of RIG-I RNA immunoprecipitation (RIP) experiments.

(B) 6×10^{13} copies of IVT-CoV-2 RNA with or without CIP treatment were used in RIG-I RIP experiments. RIG-I were equally immunoprecipitated by RIG-I antibody for CIP-treated or nontreated groups. IgG serves as a negative control (left panel). RIG-I-bound RNA was extracted by phenol-chloroform-isoamyl alcohol and purified by RNA Clean & Concentrator Kits. The purified RNA was reverse transcribed and quantified by qPCR. N = 4. Data are presented as the mean ± SEM. Group means were compared by Student's t test. **p < 0.01 and ***p < 0.001. (right panel).

(C) Graphic illustration of biotinylated RNA pull-down experiments.

(D) Biotinylated IVT-CoV-2 RNA (1×10^{14} copies) was treated with or without CIP and used in RNA pull-down assays. RNA-bound RIG-I proteins were detected by western blot.

(E) RIG-I RIP assay for SARS-CoV-2 virus from infected Caco-2 cells. 5×10^9 copies of SARS-CoV-2 viral RNA were incubated with Caco-2 cell lysates and immunoprecipitated with IgG control and anti-RIG-I antibody (left panel). IgG or RIG-I-bound RNA was extracted by phenol-chloroform-isoamyl alcohol and purified by RNA Clean & Concentrator Kits. The purified RNA was reverse transcribed and quantified by qPCR. N = 4. Data are presented as the mean ± SEM. Group means were compared by Student's t test. ***p < 0.001 (right panel).

(F) METTL3 expression in control and METTL3 KD Caco-2 cells was examined by western blotting.

(G) Equal amounts of IVT-CoV-2 RNA were transfected into control and METTL3-depleted Caco-2 cells, cell lysates were incubated with RIG-I antibody, and IP efficiency was examined by western blotting (left panel). RIG-I-bound RNA was purified and quantified as described before. N = 4. Data are presented as the mean ± SEM. Group means were compared by Student's t test. **p < 0.01 (right panel).

(H) RIG-I RIP assay for SARS-CoV-2 virus from control and METTL3 KD Caco-2 cells after SARS-CoV-2 infection. 5×10^9 copies of SARS-CoV-2 viral RNA from infected control and METTL3 KD Caco-2 cells were used for RIG-I RIP experiments. RIG-I IP efficiency was examined by western blotting. IgG serves as a negative control (left panel). RIG-I-bound RNAs were purified and quantified as described before. N = 4. Data are presented as the mean ± SEM. Group means were compared by Student's t test. *p < 0.05, **p < 0.01, and ***p < 0.001. (right panel).

See also Figure S3 and Table S4.
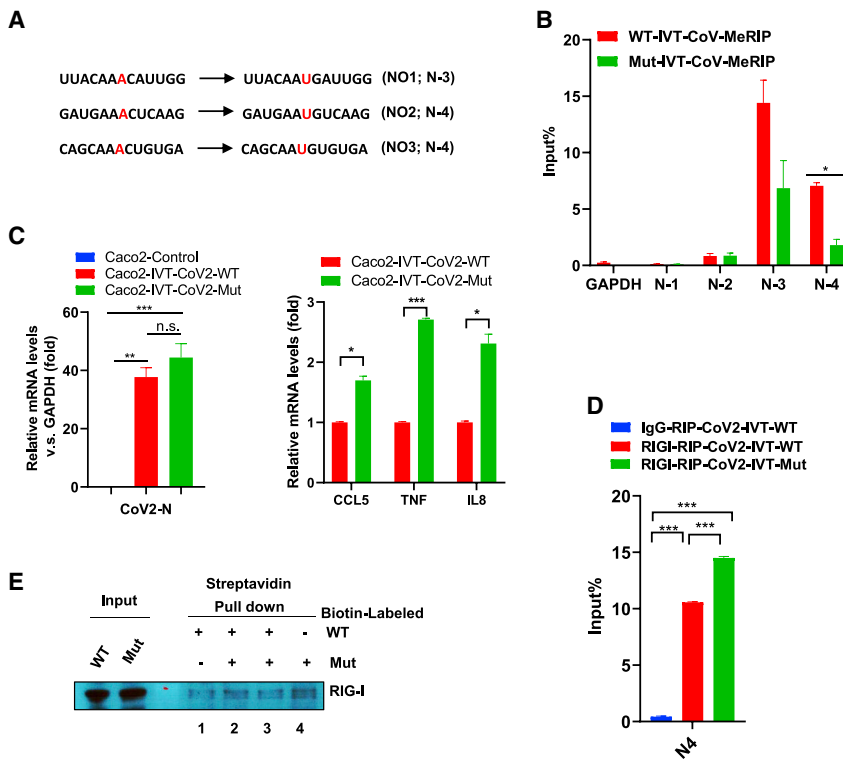
Figure 5. Mutagenesis of m6A-modified adenosine sites in SARS-CoV-2 RNA increases RIG-I recognition and inflammatory gene expression

(A) Mutagenesis of putative m6A sites in the SARS-CoV-2 N region.

(B) Equal amounts of wild-type (WT) and mutant (Mut) IVT-CoV-2 RNA were transfected into Caco-2 cells, and MeRIP-RT-qPCR was performed for WT and Mut IVT-CoV-2 RNA transfected group. N = 2. Data are presented as the mean ± SEM. Group means were compared by Student's t test. *p < 0.05.

(C) Equal amounts of WT and Mut IVT-CoV-2 RNA were transfected into Caco-2 cells. IVT-CoV-2, CCL5, TNF, and IL-8 mRNA expression was examined by qRT-PCR. N = 2. Data are presented as the mean ± SEM. Group means were compared by Student's t test. *p < 0.05, **p < 0.01, and ***p < 0.001.

(D) Equal amounts of WT and Mut IVT-CoV-2 RNA were transfected into Caco-2 cells. Cell lysates were collected, and RIG-I RIP experiments were performed by using IgG control and anti-RIG-I antibody. N = 2. Data are presented as the mean ± SEM. Group means were compared by Student's t test. ***p < 0.001.

(E) Equal amounts of biotinylated WT (lane 1) or Mut (lane 4) RNA or a mixture of WT and Mut (1:1 ratio, lanes 2 and 3) IVT-CoV-2 RNA was transfected into Caco-2 cells. Cell lysates were collected, and biotinylated RNA pull-down experiments were performed. RNA-bound RIG-I proteins were examined by western blotting.

See also Table S4.

IVT-CoV-2 RNA was increased in METTL3-depleted cells compared with control cells (Figure 4G, right panel). Next, we examined RIG-I binding of SARS-CoV-2 viral RNA from control and METTL3-depleted Caco-2 cells after infection. Consistent with IVT-CoV-2 RNA, RIG-I RIP showed that RIG-I recognition of SARS-CoV-2 RNA was significantly increased for viral RNAs obtained from METTL3-depleted cells compared with shControl cells after SARS-CoV-2 infection (Figure 4H). These results demonstrate that decreased m6A levels in SARS-CoV-2 RNA by METTL3 depletion enhanced RIG-I binding to viral RNA.

Mutation of putative m6A sites in SARS-CoV-2 RNA increased inflammation gene expression and RIG-I binding

In order to further define the role of m6A modification of SARS-CoV-2 RNA in regulating RIG-I recognition and downstream inflammatory gene induction, we generated mutations at the putative m6A-modified sites in SARS-CoV-2 RNA and analyzed their effects on downstream inflammatory gene expression and RIG-I binding capacity. Based on the N region peaks identified in our MeRIP-seq data (Tables S1 and S2), we overlapped these regions with the modified sites identified in Nanopore sequencing (Kim et al., 2020), and the modified adenosines, which were embedded in DRACH motif, were chosen for further validation (Table S1). The sequences around the three putative modified adenosine sites all have a DRACH motif. The sequences and DRACH motif are as follows: NO.1, aaAca; NO.2, aaAcu; NO.3, aaAcu; DRACH motif, D = G/A/U, R = G/A, and H = A/U/C. The putative m6A-modified site

NO.1 is located in the N-3 region, and the NO.2 and 3 sites are located in the N-4 region (Figure 5A). We generated mutants for all of these modified adenosine sites and examined m6A levels of wild-type and mutant RNAs after transfecting them into Caco-2 cells. The MeRIP-qRT-PCR results showed that mutants of the putative m6A sites resulted in reduced m6A levels in the N-3 and N-4 regions where the modified sites were located (Figures 5A and 5B). Then, we analyzed inflammation gene expression after transfecting wild-type and mutant IVT-CoV-2 RNA into Caco-2 cells and found that transfecting mutant IVT-CoV-2 RNA led to an increased inflammatory gene expression compared with wild-type RNA (Figure 5C). Lastly, we examined RIG-I binding affinity to the transfected cellular wild-type and mutant IVT-CoV-2 RNA. Both RIG-I RIP and biotinylated RNA pull-down experiments showed that mutant IVT-CoV-2 RNA enhanced RIG-I binding to RNA compared with wild-type RNA (Figures 5D and 5E). Altogether, these results showed that reduction of m6A levels of SARS-CoV-2 RNA by METTL3 depletion or mutagenesis of the m6A-modified sites enhanced RIG-I recognition and increased inflammatory gene induction.

METTL3 depletion enhances phosphorylation of IRF3 and IκBα to increase inflammatory gene expression

The above results showed that reduced m6A levels in SARS-CoV-2 viral genes by METTL3 depletion or mutagenesis of m6A sites enhanced RIG-I binding, and we wondered whether the innate immune signaling pathway and inflammatory genes downstream of RIG-I activation were affected by METTL3 KD.
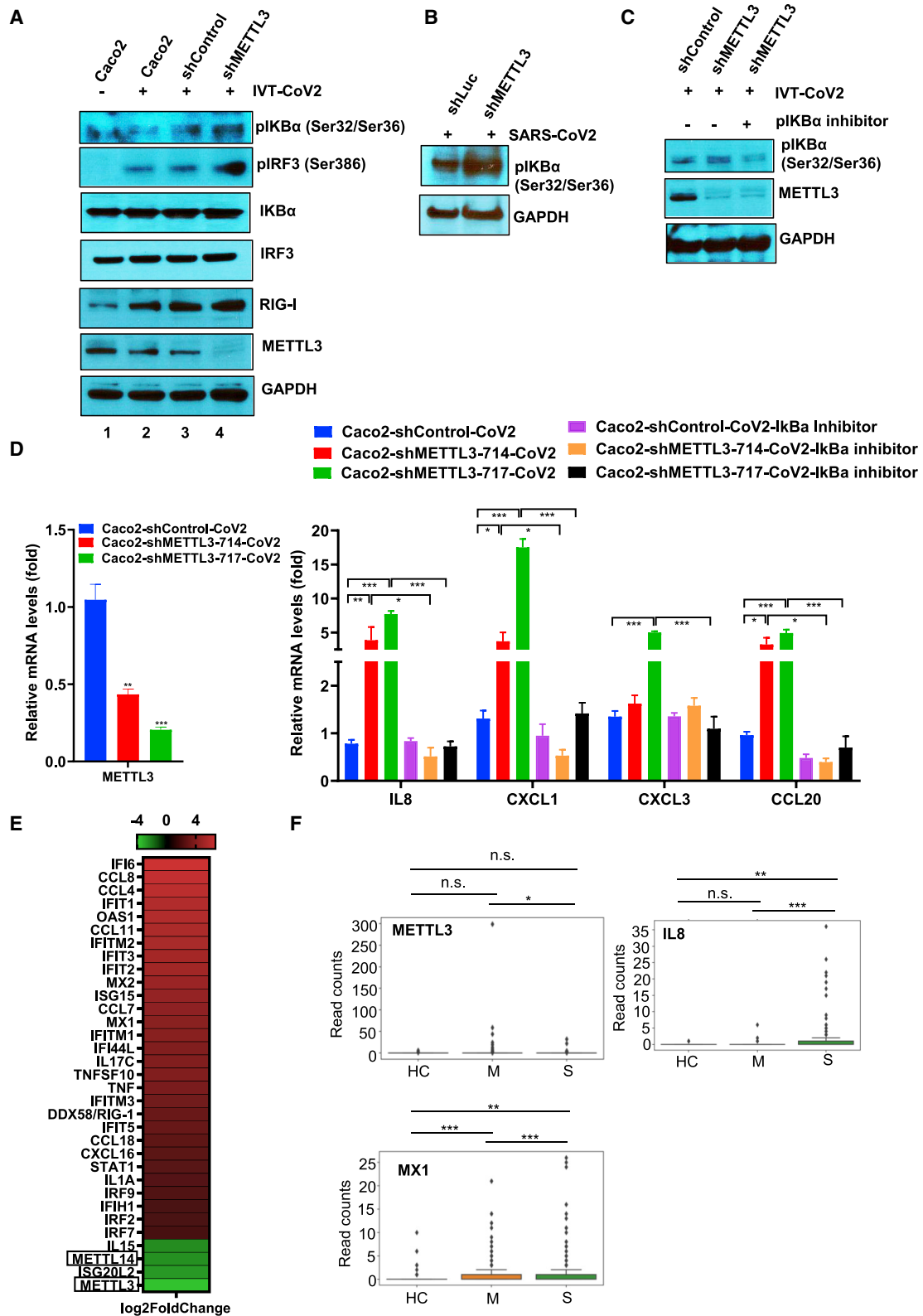
(legend on next page)

It is not fully understood which signaling pathway SARS-CoV-2 employs to stimulate the innate immune response. Based on a previous report (Jensen and Thomsen, 2012), we hypothesized that IRF3 and nuclear factor κB (NF-κB) are two of the key molecules mediating the activation of downstream gene expression.

We examined activation of the RLR innate immune signaling pathway by analyzing protein expression of IRF3, IκBα, RIG-I, and METTL3 and phosphorylation of IRF3 and IκBα. After transfecting IVT CoV-2 RNA, protein expression of RIG-I and phosphorylation of IRF3 were increased when compared with parental cells without transfection of IVT CoV-2 RNA, suggesting an activation of the RIG-I pathway after introducing exogenous CoV-2 RNAs to cells (lanes 1 and 2 in Figure 6A). Next, we examined the effects of METTL3 on the activation of the innate immune signaling pathway after IVT CoV-2 RNA transfection. METTL3 depletion did not alter RIG-I expression levels, while phosphorylation of IRF3 and IκBα were increased compared with control cells transfecting IVT CoV-2 RNA (lanes 3 and 4 in Figure 6A). These results suggest that METTL3 depletion enhanced phosphorylation of IRF3 and IκBα to increase downstream innate immune effector gene expression, as we observed in live virus infection experiments (Figures 3C and 3D). As we observed increased inflammatory gene expression in METTL3-depleted Caco-2 cells during SARS-CoV-2 infection, and because they are the downstream effectors of RIG-I and NF-κB activation, we examined phosphorylation of IκBα in control and METTL3 KD Caco-2 cells during SARS-CoV-2 infection. Similarly, METTL3 depletion enhanced phosphorylation of IκBα during SARS-CoV-2 infection (Figure 6B).

We further confirmed the role of NF-κB activation in inducing inflammatory cytokine/chemokine expression in METTL3 KD cells after IVT CoV-2 RNA transfection by adding a specific IκBα phosphorylation inhibitor. After transfection with IVT CoV-2 RNA, METTL3-depleted cells were treated with or without the IκBα phosphorylation inhibitor Bay 11-7083 (Hu et al., 2001; Pierce et al., 1997). We found that IκBα phosphorylation inhibitor diminished the enhancement of IκBα phosphorylation by METTL3 depletion after IVT CoV RNA transfection (Figure 6C). Next, we performed live viral experiments by comparing the expression of downstream inflammatory targets in control and METTL3-depleted cells with or without adding the IκBα phos-

phorylation inhibitor during SARS-CoV-2 infection. To avoid off-target effects, we used two different shRNAs to knock down METTL3 during SARS-CoV-2 infection. METTL3 KD increased IL-8, CXCL1, CXCL3, and CCL20 gene expression compared with control cells during SARS-CoV-2 infection, and the increase in gene expression correlated with METTL3 KD efficacy (Figure 6D). In addition, the IκBα phosphorylation inhibitor decreased inflammatory gene induction by METTL3 depletion during SARS-CoV-2 infection. These results showed that METTL3 depletion increases phosphorylation of IRF3 and IκBα compared with shControl, and NF-κB activation is the upstream event of inflammatory gene induction in METTL3-depleted Caco-2 cells during SARS-CoV-2 infection.

METTL3 expression is reduced and inflammatory genes are induced in severe COVID-19 patients

To validate our findings in COVID-19 patients, we analyzed DEGs in post-mortem lung samples of COVID-19 patients compared with healthy lung biopsy specimens (Blanco-Melo et al., 2020). Our bioinformatics analysis results showed that most of the inflammatory genes and ISGs were increased in the COVID-19 patients compared with healthy lung samples, while METTL3 and METTL14 gene expression was significantly downregulated (Figure 6E). Furthermore, we analyzed the single-cell RNA-seq data of epithelial cells from bronchoalveolar lavage fluid (BALF) of healthy controls (HCs) and COVID-19 patients with moderate (M) or severe (S) disease (Liao et al., 2020). Our data showed that METTL3 levels were significantly decreased in epithelial cells of severe COVID-19 patients compared with moderate disease states, and correspondingly, the inflammatory gene IL-8 and the ISG MX1 were significantly increased in patients with severe disease (Figure 6F). Altogether, these results show that the reduction of host m6A methyltransferase METTL3 and/or METTL14 gene expression in severe COVID-19 patients was accompanied by increased inflammatory gene expression, which may corroborate with our findings and the proposed mechanism obtained in cellular models. The exact relationship of m6A methyltransferases and increased inflammation in COVID-19 patients needs further investigation.

In summary, our results showed that (1) SARS-CoV-2 virus has a m6A modification enriched in the N region; (2) METTL3 depletion

---

Figure 6. METTL3 depletion leads to increased IRF3 and IκBα phosphorylation and inflammatory gene expression

(A) Mock-transfected Caco-2 cells or Caco-2 cells (Caco-2, shControl, or shMETTL3) transfected with equal amounts of IVT-SARS-CoV-2-N RNA were collected for western blotting.

(B) Phosphorylation levels of IκBα were determined in shControl and METTL3-depleted Caco-2 cells upon SARS-CoV-2 infection by western blotting.

(C) shControl and METTL3-depleted Caco-2 cells were transfected with equal amounts of IVT-SARS-CoV-2-N RNA, and METTL3-depleted cells were treated with or without IκBα phosphorylation inhibitor Bay 11-7083. IκBα phosphorylation and METTL3 levels were examined by western blot.

(D) shControl or METTL3 KD Caco-2 cells were infected with SARS-CoV-2 virus and treated with or without the IκBα phosphorylation inhibitor Bay 11-7083, and cells were then collected for RNA extraction. Expression levels of the inflammatory genes IL-8, CXCL1, CXCL3, and CCL20 were compared between control and METTL3 KD cells as well as cells treated with or without IκBα phosphorylation inhibitor upon SARS-CoV-2 infection (right panel). Two shRNAs were used to knock down METTL3, and KD efficacy was examined by qRT-PCR (left panel). N = 3. Data are presented as the mean ± SEM. Group means were compared by Student's t test. *p < 0.05, **p < 0.01, and ***p < 0.001.

(E) Significantly changed genes from lung samples of COVID-19 patients compared with healthy controls (Blanco-Melo et al., 2020). Inflammatory genes and ISGs, as well as METTL3 and METTL14, are shown as log2 (fold change). The genes shown have the p adj < 0.05 and pass the Wald test for the gene counts.

(F) Bar graphs of METTL3, IL-8, and MX1 expression in healthy controls (HCs) and COVID-19 patients with moderate (M) or severe (S) disease (Liao et al., 2020). Single-cell RNA expression from epithelial cells of bronchoalveolar lavage fluid (BALF) from healthy donor and COVID-19-infected patients was analyzed, and the difference between each group was compared. Data are presented as the mean ± SEM. Group means were compared by Student's t test. n.s., not significant; *p < 0.05, **p < 0.01, and ***p < 0.001.

See also Table S4.
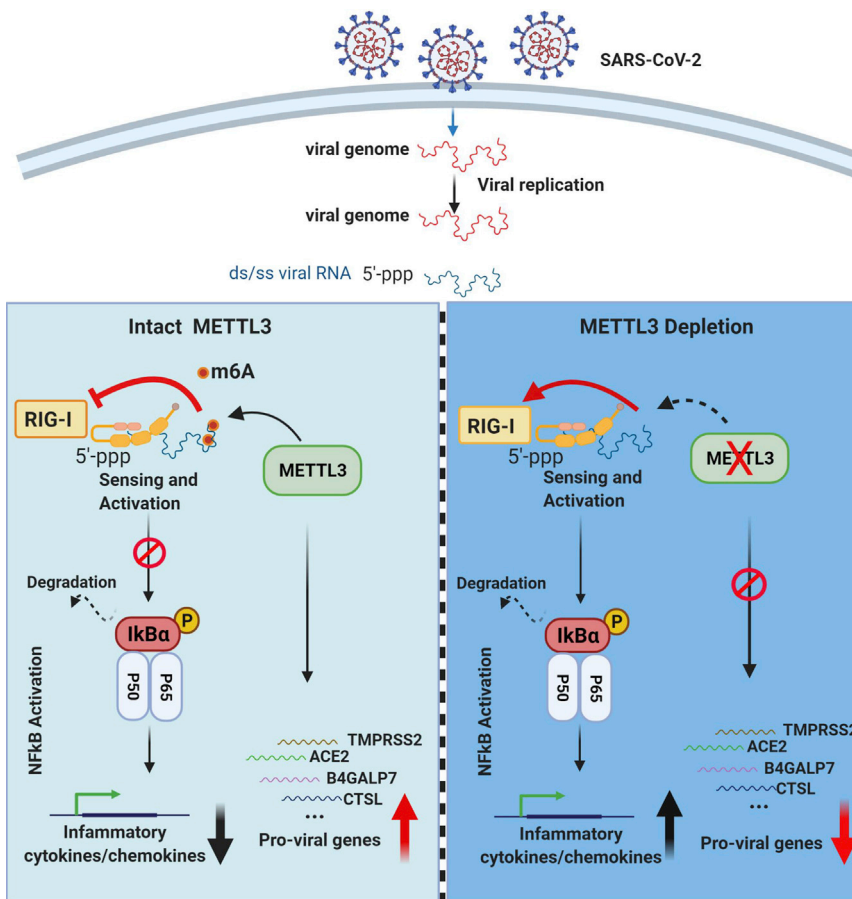
Figure 7. SARS-CoV-2 virus utilizes the host m6A methyltransferase METTL3 to modify viral RNA and evade host innate immune responses

(Left) After entry into the host cell, the viral genome enters the replication phase, and 5′-phosphorylated viral RNA is generated, which is m6A modified by METTL3 and does not bind RIG-I to activate immune pathways. Viral infection also enhances METTL3-mediated proviral gene expression. (Right) When METTL3 is depleted, m6A levels of viral RNA are reduced, and RIG-I-bound viral RNA is increased, leading to enhanced RIG-I sensing and activation, which is followed by downstream activation of the NF-κB pathway and inflammatory gene expression. In addition, METTL3 depletion alters gene expression and m6A levels of several proviral host factors upon SARS-CoV-2 infection.

reduces m6A levels in SARS-CoV-2 gene; (3) METTL3 depletion reduces SARS-CoV-2 viral load, proviral gene expression, and m6A levels in host cells during viral infection in Caco-2 cells; (4) m6A reduction in viral gene increases RIG-I binding and subsequently enhances the downstream innate immune signaling pathway and inflammatory gene expression; and (5) expression of m6A methyltransferase METTL3 is reduced and inflammatory gene expression is increased in severe COVID-19 patients (Figure 7).

DISCUSSION

Innate immune sensing and response to viral entry into a host cell is critical for host antiviral defense by inducing IFN and inflammatory cytokines and chemokines. A rapid and effective innate immune response is important to restrict viral replication and activate the viral-specific adaptive immune response. However, excessive proinflammatory cytokines and chemokines (e.g., IL-6, IL-8, IL-1, CXCL10/IP10, and TNFα) play a pivotal role in the pathogenesis of COVID-19, such as acute lung injury (ALI) and ARDS in infected patients (Qin et al., 2020; Xu et al., 2020). Therefore, it is urgent and important to investigate the factors and signaling pathways contributing to the immune response of host cells to SARS-CoV-2 infection.

Viral RNA modifications play important roles for viruses to evade innate immune recognition and response by their own

evolved enzymes or utilizing host cell enzymes to modify the viral RNA and make it undistinguishable from the host cell RNAs (Durbin et al., 2016; Karikó et al., 2005; Lu et al., 2020a). m6A modifications and m6A methyltransferases were reported to be essential for the RNA virus life cycle and host cell response (Courtney et al., 2017; Gokhale et al., 2020; Hao et al., 2019; Huang et al., 2018; Lang et al., 2019; Lichinchi et al., 2016a, 2016b; Rubio et al., 2018; Tirumuru et al., 2016; Winkler et al., 2019; Xue et al., 2019). SARS-CoV-2 is a positive-sense RNA virus belonging to the β-coronavirus genus (Lu et al., 2020b). A recent report using Nanopore direct sequencing suggested that SARS-CoV-2 RNA was modified, but no modification types were identified (Kim et al., 2020). We further examined the modified sites and the surrounding motif reported by Kim et al. (2020). From the 41 identified modified sites, 20 modified sites belong to the "AAGAA-like" motif as reported in the study. More than half of the modified sites were excluded from the AAGAA motif, among which we observed modified adenosine sites embedded in the DRACH motif (D = G/A/U, R = G/A, H = A/U/C), indicating the existence of m6A modification in the viral genome (Table S1). We incorporated three modified adenosine sites embedded in the DRACH motif identified by the Nanopore study with our MeRIP data, and mutagenesis of the three sites showed decreased levels of m6A in the mutant RNA (Figure 5). In addition, SARS-CoV-2 viral m6A levels decreased in infected METTL3 KD cells at the same region (Figure 1). These data support and validate the identification of m6A modification in SARS-CoV-2 virus.

In this study, we discovered that SARS-CoV-2 RNA contains diverse chemical modifications. We observed the presence of m6A modifications in SARS-CoV-2 virus and further identified that the m6A-modified sites were enriched in the N region of the SARS-CoV-2 genome. Furthermore, we studied the function of m6A modification in the host innate immune response by

depleting the host cell m6A methyltransferase METTL3 after SARS-CoV-2 infection. Depleting METTL3 enhanced innate immune effector gene expression, suggesting that reduced m6A levels in SARS-CoV-2 RNA may increase host cell immunity to viral infection. To delineate the role and mechanisms of m6A modification in SARS-CoV-2 affecting the host cell innate immune response, we chose both SARS-CoV-2 virus and the IVT-SARS-CoV-2 N region, which has enriched m6A sites and SARS-CoV-2 virus, to analyze the mechanism. We found that m6A levels of SARS-CoV-2 RNA were reduced by METTL3 depletion, and RIG-I binding to the viral gene was increased. Furthermore, mutagenesis of the putative modified m6A sites also increased RIG-I binding to cellular CoV-2 RNA and inflammatory gene expression. Increased RIG-I binding of SARS-CoV-2 viral RNA activated IκBα phosphorylation and enhanced downstream inflammatory gene expression in METTL3-depleted cells after SARS-CoV-2 infection or transfection of IVT-CoV-2 RNA.

In summary, our study investigated the RNA modification profile of SARS-CoV-2 virus and focused on m6A modification and its functional relevance to the host cell innate immune response. We uncovered a new mechanism of SARS-CoV-2 utilizing host cell m6A methyltransferase to modify its RNA, evade innate immune recognition, and regulate the activation of downstream inflammatory genes. These findings enhance our understanding of COVID-19 pathogenesis and would help future studies to regulate the innate immune response to SARS-CoV-2 infection in a more precise and time-dependent manner in order to achieve a balance of essential innate immune responses and avoid the excessive activation of inflammatory genes.

Furthermore, we observed that METTL3 depletion in Caco-2 cells reduced viral loads after SARS-CoV-2 infection, and RNA-seq analysis showed that the DEGs belonged to multiple important biological processes, which were reported to affect the SARS-CoV-2 life cycle and viral replication (Bojkova et al., 2020; Gordon et al., 2020). METTL3 may regulate host factors that affect multiple stages of the SARS-CoV-2 life cycle and viral replication. Therefore, we examined the expression of identified SARS-CoV-2 proviral host genes in control and METTL3-depleted Caco-2 cells during viral infection. METTL3 depletion reduced mRNA expression and m6A levels of several proviral host genes during SARS-CoV-2 infection. The combined effects of directly regulating m6A levels in the virus to enhance a timely innate immune response and indirectly perturbing the viral life cycle by METTL3 depletion/inhibition may benefit the treatment of COVID-19 patients, especially for patients with mild or moderate disease who have not developed a cytokine storm.

Limitations of study

In the current study, we found that METTL3 depletion reduced expression and m6A levels of several proviral genes during SARS-CoV-2 infection. The exact mechanisms underlying the altered host factors and viral replication regulated by METTL3 depletion during SARS-CoV-2 infection will need further investigation. It will be important to determine the molecular mechanisms of essential gene expression that are involved in the SARS-CoV-2 life cycle and host immunity. As RIG-I is the highly expressed upstream RLR/TLR in Caco-2 cells during SARS-

CoV-2 infection, and Caco-2 cells are more sensitive to RIG-I-specific PAMP RNA (Table S3; Figures S3G–S3I), we focused our study on the mechanism of m6A in affecting RIG-I recognition upon SARS-CoV-2 infection, which does not exclude the functions of other RLR/TLR sensors in mediating the innate immune response in other contexts or cell types. We assessed the role of RIG-I in regulating innate immune responses through sensing m6A levels in SARS-CoV-2 RNA by using *in vitro* cellular models for RIG-I recognition of IVT RNA or SARS-CoV-2 virus as well as IVT SARS-CoV-2 m6A mutants (Figures 4 and 5). Further viral infection studies using m6A sites mutated in the context of the full-length viral genome and RIG-I loss of function will be helpful to test the model proposed in Figure 7. In addition, future studies to validate the cellular results in animal models infected by SARS-CoV-2 or other viruses will be helpful to link the mechanisms of gene expression and syndromes found in human COVID-19 patients.

STAR★METHODS

Detailed methods are provided in the online version of this paper and include the following:

- KEY RESOURCES TABLE
- RESOURCE AVAILABILITY
  - Lead contact
  - Materials availability
  - Data and code availability
- EXPERIMENTAL MODEL AND SUBJECT DETAILS
  - Cell lines and virus strain
- METHOD DETAILS
  - Generation of knockdown cell lines
  - SARS-CoV-2 viral infection, SARS-CoV-2-N IVT RNA production, transfection, and inhibitor treatment
  - MeRIP-seq and MeRIP-RT qPCR of SARS-CoV-2 virus
  - MeRIP-seq data analysis
  - RNA-seq and data analysis
  - RT-qPCR
  - Western blot analysis
  - RNA immunoprecipitation (RIP)
  - Biotinylated RNA pulldown assay
  - LC-MS/MS/MS quantification of SARS-CoV-2 RNA modifications
- QUANTIFICATION AND STATISTICAL ANALYSIS

SUPPLEMENTAL INFORMATION

Supplemental information can be found online at https://doi.org/10.1016/j.celrep.2021.109091.

REFERENCES

Akira, S., Uematsu, S., and Takeuchi, O. (2006). Pathogen recognition and innate immunity. Cell *124*, 783–801.

Blanco-Melo, D., Nilsson-Payant, B.E., Liu, W.C., Uhl, S., Hoagland, D., Møller, R., Jordan, T.X., Oishi, K., Panis, M., Sachs, D., et al. (2020). Imbalanced Host Response to SARS-CoV-2 Drives Development of COVID-19. Cell *181*, 1036–1045.e9.

Bojkova, D., Klann, K., Koch, B., Widera, M., Krause, D., Ciesek, S., Cinatl, J., and Münch, C. (2020). Proteomics of SARS-CoV-2-infected host cells reveals therapy targets. Nature *583*, 469–472.

Brubaker, S.W., Bonham, K.S., Zanoni, I., and Kagan, J.C. (2015). Innate immune pattern recognition: a cell biological perspective. Annu. Rev. Immunol. *33*, 257–290.

Cantuti-Castelvetri, L., Ojha, R., Pedro, L.D., Djannatian, M., Franz, J., Kuivanen, S., van der Meer, F., Kallio, K., Kaya, T., Anastasina, M., et al. (2020). Neuropilin-1 facilitates SARS-CoV-2 cell entry and infectivity. Science *370*, 856–860.

Catanzaro, M., Fagiani, F., Racchi, M., Corsini, E., Govoni, S., and Lanni, C. (2020). Immune response in COVID-19: addressing a pharmacological challenge by targeting pathways triggered by SARS-CoV-2. Signal Transduct. Target. Ther. *5*, 84.

Clausen, T.M., Sandoval, D.R., Spliid, C.B., Pihl, J., Perrett, H.R., Painter, C.D., Narayanan, A., Majowicz, S.A., Kwong, E.M., McVicar, R.N., et al. (2020). SARS-CoV-2 Infection Depends on Cellular Heparan Sulfate and ACE2. Cell *183*, 1043–1057.e15.

Courtney, D.G., Kennedy, E.M., Dumm, R.E., Bogerd, H.P., Tsai, K., Heaton, N.S., and Cullen, B.R. (2017). Epitranscriptomic Enhancement of Influenza A Virus Gene Expression and Replication. Cell Host Microbe *22*, 377–386.e5.

Daniloski, Z., Jordan, T.X., Wessels, H.H., Hoagland, D.A., Kasela, S., Legut, M., Maniatis, S., Mimitou, E.P., Lu, L., Geller, E., et al. (2021). Identification of Required Host Factors for SARS-CoV-2 Infection in Human Cells. Cell *184*, 92–105.e16.

Durbin, A.F., Wang, C., Marcotrigiano, J., and Gehrke, L. (2016). RNAs Containing Modified Nucleotides Fail To Trigger RIG-I Conformational Changes for Innate Immune Signaling. MBio *7*, e00833-16.

Fu, L., Amato, N.J., Wang, P., McGowan, S.J., Niedernhofer, L.J., and Wang, Y. (2015). Simultaneous Quantification of Methylated Cytidine and Adenosine in Cellular and Tissue RNA by Nano-Flow Liquid Chromatography-Tandem Mass Spectrometry Coupled with the Stable Isotope-Dilution Method. Anal. Chem. *87*, 7653–7659.

Gokhale, N.S., McIntyre, A.B.R., McFadden, M.J., Roder, A.E., Kennedy, E.M., Gandara, J.A., Hopcraft, S.E., Quicke, K.M., Vazquez, C., Willer, J., et al. (2016). N6-Methyladenosine in Flaviviridae Viral RNA Genomes Regulates Infection. Cell Host Microbe *20*, 654–665.

Gokhale, N.S., McIntyre, A.B.R., Mattocks, M.D., Holley, C.L., Lazear, H.M., Mason, C.E., and Horner, S.M. (2020). Altered m6A Modification of Specific Cellular Transcripts Affects Flaviviridae Infection. Mol. Cell *77*, 542–555.e8.

Gonzalez, G., Cui, Y., Wang, P., and Wang, Y. (2020). Normalized retention time for scheduled liquid chromatography-multistage mass spectrometry analysis of epitranscriptomic modifications. J. Chromatogr. A *1623*, 461181.

Gordon, D.E., Jang, G.M., Bouhaddou, M., Xu, J., Obernier, K., White, K.M., O'Meara, M.J., Rezelj, V.V., Guo, J.Z., Swaney, D.L., et al. (2020). A SARS-CoV-2 protein interaction map reveals targets for drug repurposing. Nature *583*, 459–468.

Hao, H., Hao, S., Chen, H., Chen, Z., Zhang, Y., Wang, J., Wang, H., Zhang, B., Qiu, J., Deng, F., and Guan, W. (2019). N6-methyladenosine modification and METTL3 modulate enterovirus 71 replication. Nucleic Acids Res. *47*, 362–374.

Hoffmann, M., Kleine-Weber, H., Schroeder, S., Krüger, N., Herrler, T., Erichsen, S., Schiergens, T.S., Herrler, G., Wu, N.H., Nitsche, A., et al. (2020). SARS-CoV-2 Cell Entry Depends on ACE2 and TMPRSS2 and Is Blocked by a Clinically Proven Protease Inhibitor. Cell *181*, 271–280.e8.

Hu, X., Janssen, W.E., Moscinski, L.C., Bryington, M., Dangsupa, A., Rezai-Zadeh, N., Babbin, B.A., and Zuckerman, K.S. (2001). An IkappaBalpha inhibitor causes leukemia cell death through a p38 MAP kinase-dependent, NF-kappaB-independent mechanism. Cancer Res. *61*, 6290–6296.

Huang, H., Weng, H., Sun, W., Qin, X., Shi, H., Wu, H., Zhao, B.S., Mesquita, A., Liu, C., Yuan, C.L., et al. (2018). Recognition of RNA N6-methyladenosine by IGF2BP proteins enhances mRNA stability and translation. Nat. Cell Biol. *20*, 285–295.

Huang, C., Wang, Y., Li, X., Ren, L., Zhao, J., Hu, Y., Zhang, L., Fan, G., Xu, J., Gu, X., et al. (2020). Clinical features of patients infected with 2019 novel coronavirus in Wuhan, China. Lancet *395*, 497–506.

Hui, K.P.Y., Cheung, M.C., Perera, R.A.P.M., Ng, K.C., Bui, C.H.T., Ho, J.C.W., Ng, M.M.T., Kuok, D.I.T., Shih, K.C., Tsao, S.W., et al. (2020). Tropism, replication competence, and innate immune responses of the coronavirus SARS-CoV-2 in human respiratory tract and conjunctiva: an analysis in ex-vivo and in-vitro cultures. Lancet Respir. Med. *8*, 687–695.

Jensen, S., and Thomsen, A.R. (2012). Sensing of RNA viruses: a review of innate immune receptors involved in recognizing RNA virus invasion. J. Virol. *86*, 2900–2910.

Karikó, K., Buckstein, M., Ni, H., and Weissman, D. (2005). Suppression of RNA recognition by Toll-like receptors: the impact of nucleoside modification and the evolutionary origin of RNA. Immunity *23*, 165–175.

Kell, A.M., and Gale, M., Jr. (2015). RIG-I in RNA virus recognition. Virology *479-480*, 110–121.

Kim, G.W., Imam, H., Khan, M., and Siddiqui, A. (2020). N^6-Methyladenosine modification of hepatitis B and C viral RNAs attenuates host innate immunity via RIG-I signaling. J. Biol. Chem. *295*, 13123–13133.

Krafcikova, P., Silhan, J., Nencka, R., and Boura, E. (2020). Structural analysis of the SARS-CoV-2 methyltransferase complex involved in RNA cap creation bound to sinefungin. Nat. Commun. *11*, 3717.

Lang, F., Singh, R.K., Pei, Y., Zhang, S., Sun, K., and Robertson, E.S. (2019). EBV epitranscriptome reprogramming by METTL14 is critical for viral-associated tumorigenesis. PLoS Pathog. *15*, e1007796.

Lei, X., Dong, X., Ma, R., Wang, W., Xiao, X., Tian, Z., Wang, C., Wang, Y., Li, L., Ren, L., et al. (2020). Activation and evasion of type I interferon responses by SARS-CoV-2. Nat. Commun. *11*, 3810.

Li, J., Liu, Y., and Zhang, X. (2010). Murine coronavirus induces type I interferon in oligodendrocytes through recognition by RIG-I and MDA5. J. Virol. *84*, 6472–6482.

Li, N., Kang, Y., Wang, L., Huff, S., Tang, R., Hui, H., Agrawal, K., Gonzalez, G.M., Wang, Y., Patel, S.P., and Rana, T.M. (2020). ALKBH5 regulates anti-PD-1 therapy response by modulating lactate and suppressive immune cell accumulation in tumor microenvironment. Proc. Natl. Acad. Sci. USA *117*, 20159–20170.

Liao, M., Liu, Y., Yuan, J., Wen, Y., Xu, G., Zhao, J., Cheng, L., Li, J., Wang, X., Wang, F., et al. (2020). Single-cell landscape of bronchoalveolar immune cells in patients with COVID-19. Nat. Med. *26*, 842–844.

Lichinchi, G., and Rana, T.M. (2019). Profiling of N^6-Methyladenosine in Zika Virus RNA and Host Cellular mRNA. Methods Mol. Biol. *1870*, 209–218.

Lichinchi, G., Gao, S., Saletore, Y., Gonzalez, G.M., Bansal, V., Wang, Y., Mason, C.E., and Rana, T.M. (2016a). Dynamics of the human and viral m(6)A RNA methylomes during HIV-1 infection of T cells. Nat. Microbiol. *1*, 16011.

Lichinchi, G., Zhao, B.S., Wu, Y., Lu, Z., Qin, Y., He, C., and Rana, T.M. (2016b). Dynamics of Human and Viral RNA Methylation during Zika Virus Infection. Cell Host Microbe *20*, 666–673.

Loo, Y.M., and Gale, M., Jr. (2011). Immune signaling by RIG-I-like receptors. Immunity *34*, 680–692.

Lu, M., Zhang, Z., Xue, M., Zhao, B.S., Harder, O., Li, A., Liang, X., Gao, T.Z., Xu, Y., Zhou, J., et al. (2020a). N^6-methyladenosine modification enables viral RNA to escape recognition by RNA sensor RIG-I. Nat. Microbiol. *5*, 584–598.

Lu, R., Zhao, X., Li, J., Niu, P., Yang, B., Wu, H., Wang, W., Song, H., Huang, B., Zhu, N., et al. (2020b). Genomic characterisation and epidemiology of 2019 novel coronavirus: implications for virus origins and receptor binding. Lancet *395*, 565–574.

McIntyre, W., Netzband, R., Bonenfant, G., Biegel, J.M., Miller, C., Fuchs, G., Henderson, E., Arra, M., Canki, M., Fabris, D., and Pager, C.T. (2018). Positive-sense RNA viruses reveal the complexity and dynamics of the cellular and viral epitranscriptomes during infection. Nucleic Acids Res. *46*, 5776–5791.

Peritz, T., Zeng, F., Kannanayakal, T.J., Kilk, K., Eiríksdóttir, E., Langel, U., and Eberwine, J. (2006). Immunoprecipitation of mRNA-protein complexes. Nat. Protoc. *1*, 577–580.

Pierce, J.W., Schoenleber, R., Jesmok, G., Best, J., Moore, S.A., Collins, T., and Gerritsen, M.E. (1997). Novel inhibitors of cytokine-induced IkappaBalpha phosphorylation and endothelial cell adhesion molecule expression show anti-inflammatory effects in vivo. J. Biol. Chem. *272*, 21096–21103.

Qin, C., Zhou, L., Hu, Z., Zhang, S., Yang, S., Tao, Y., Xie, C., Ma, K., Shang, K., Wang, W., et al. (2020). Dysregulation of immune response in patients with COVID-19 in Wuhan, China. Clin. Infect. Dis. *71*, 762–768.

Rubio, R.M., Depledge, D.P., Bianco, C., Thompson, L., and Mohr, I. (2018). RNA m^{6}A modification enzymes shape innate responses to DNA by regulating interferon β. Genes Dev. *32*, 1472–1484.

Tirumuru, N., Zhao, B.S., Lu, W., Lu, Z., He, C., and Wu, L. (2016). N(6)-methyladenosine of HIV-1 RNA regulates viral infection and HIV-1 Gag protein expression. eLife *5*, e15528.

Tiwari, S.K., Wang, S., Smith, D., Carlin, A.F., and Rana, T.M. (2021). Revealing Tissue-Specific SARS-CoV-2 Infection and Host Responses using Human Stem Cell-Derived Lung and Cerebral Organoids. Stem Cell Reports *16*, 437–445.

Totura, A.L., and Baric, R.S. (2012). SARS coronavirus pathogenesis: host innate immune responses and viral antagonism of interferon. Curr. Opin. Virol. *2*, 264–275.

Wang, Y., Ludwig, J., Schuberth, C., Goldeck, M., Schlee, M., Li, H., Juranek, S., Sheng, G., Micura, R., Tuschl, T., et al. (2010). Structural and functional insights into 5′-ppp RNA pattern recognition by the innate immune receptor RIG-I. Nat. Struct. Mol. Biol. *17*, 781–787.

Wang, X., Lu, Z., Gomez, A., Hon, G.C., Yue, Y., Han, D., Fu, Y., Parisien, M., Dai, Q., Jia, G., et al. (2014). N6-methyladenosine-dependent regulation of messenger RNA stability. Nature *505*, 117–120.

Wang, L., Hui, H., Agrawal, K., Kang, Y., Li, N., Tang, R., Yuan, J., and Rana, T.M. (2020a). m^{6}A RNA methyltransferases METTL3/14 regulate immune responses to anti-PD-1 therapy. EMBO J. *39*, e104514.

Wang, S., Li, W., Hui, H., Tiwari, S.K., Zhang, Q., Croker, B.A., Rawlings, S., Smith, D., Carlin, A.F., and Rana, T.M. (2020b). Cholesterol 25-Hydroxylase inhibits SARS-CoV-2 and other coronaviruses by depleting membrane cholesterol. EMBO J. *39*, e106057.

Wei, J., Alfajaro, M.M., DeWeirdt, P.C., Hanna, R.E., Lu-Culligan, W.J., Cai, W.L., Strine, M.S., Zhang, S.M., Graziano, V.R., Schmitz, C.O., et al. (2021). Genome-wide CRISPR Screens Reveal Host Factors Critical for SARS-CoV-2 Infection. Cell *184*, 76–91.

Winkler, R., Gillis, E., Lasman, L., Safra, M., Geula, S., Soyris, C., Nachshon, A., Tai-Schmiedel, J., Friedman, N., Le-Trilling, V.T.K., et al. (2019). m^{6}A modification controls the innate immune response to infection by targeting type I interferons. Nat. Immunol. *20*, 173–182.

Xia, H., Cao, Z., Xie, X., Zhang, X., Chen, J.Y., Wang, H., Menachery, V.D., Rajsbaum, R., and Shi, P.Y. (2020). Evasion of Type I Interferon by SARS-CoV-2. Cell Rep. *33*, 108234.

Xu, Z., Shi, L., Wang, Y., Zhang, J., Huang, L., Zhang, C., Liu, S., Zhao, P., Liu, H., Zhu, L., et al. (2020). Pathological findings of COVID-19 associated with acute respiratory distress syndrome. Lancet Respir. Med. *8*, 420–422.

Xue, M., Zhao, B.S., Zhang, Z., Lu, M., Harder, O., Chen, P., Lu, Z., Li, A., Ma, Y., Xu, Y., et al. (2019). Viral N^6-methyladenosine upregulates replication and pathogenesis of human respiratory syncytial virus. Nat. Commun. *10*, 4595.

Yuen, C.K., Lam, J.Y., Wong, W.M., Mak, L.F., Wang, X., Chu, H., Cai, J.P., Jin, D.Y., To, K.K., Chan, J.F., et al. (2020). SARS-CoV-2 nsp13, nsp14, nsp15 and orf6 function as potent interferon antagonists. Emerg. Microbes Infect. *9*, 1418–1428.

Zang, R., Gomez Castro, M.F., McCune, B.T., Zeng, Q., Rothlauf, P.W., Sonnek, N.M., Liu, Z., Brulois, K.F., Wang, X., Greenberg, H.B., et al. (2020). TMPRSS2 and TMPRSS4 promote SARS-CoV-2 infection of human small intestinal enterocytes. Sci. Immunol. *5*, eabc3582.

Zhou, P., Yang, X.L., Wang, X.G., Hu, B., Zhang, L., Zhang, W., Si, H.R., Zhu, Y., Li, B., Huang, C.L., et al. (2020). A pneumonia outbreak associated with a new coronavirus of probable bat origin. Nature *579*, 270–273.

STAR★METHODS

KEY RESOURCES TABLE

REAGENT or RESOURCE	SOURCE	IDENTIFIER
Antibodies		
Rabbit polyclonal anti-RIG-I	Proteintech	Cat# 20566-1-AP, RRID:AB_10700006)
Mouse monoclonal anti-RIG-I	MilliporeSigma	Cat# MABF297, RRID:AB_2650546
Rabbit monoclonal anti-IRF-3	Cell Signaling Technology	Cat# 11904, RRID:AB_2722521
Mouse monoclonal anti-IκBα	Cell Signaling Technology	Cat# 4814, RRID:AB_390781
Rabbit monoclonal anti-Phospho-IRF-3 (Ser386)	Cell Signaling Technology	Cat# 37829, RRID:AB_2799121
Mouse monoclonal anti-Phospho-IκBα (Ser32/36)	Cell Signaling Technology	Cat# 9246, RRID:AB_2267145)
Rabbit polyclonal anti-METTL3	Proteintech	Cat# 15073-1-AP, RRID:AB_2142033
Rabbit monoclonal anti-GAPDH	Cell Signaling Technology	Cat# 2118, RRID:AB_561053
Bacterial and virus strains		
SARS-CoV-2 virus	BEI Resources	USA-WA1/2020
Chemicals, peptides, and recombinant proteins		N/A
Pierce Protein A/G Magnetic Beads	Thermo Fisher	88802
Lipofectamine 3000	Thermo Fisher	L3000015
puromycin	Alfa Aesar	53-79-2
Ambion RNA Fragmentation Reagent	Thermo Fisher	AM8740
N6-Methyladenosine (m6A)	abcam	ab145715
Bay 11-7085	R&D Systems	1743/10
TRIzol LS Reagent	Thermo Fisher	10296010
TRIzol Reagent	Thermo Fisher	15596026
Streptavidin magnetic Beads	NEB	S1420S
Critical commercial assays		
RNA Clean & Concentrator-5	ZYMO RESEARCH	R1013
RNA Clean & Concentrator-25	ZYMO RESEARCH	R1018
MEGAscript T7 Transcription Kit	Thermo Fisher	AMB13345
mMESSAGE T7 Transcription Kit	Thermo Fisher	AM1344
Direct-zol RNA Kit	ZYMO RESEARCH	R2052
Quick-RNA Miniprep Plus Kit	ZYMO RESEARCH	R1055
iScript cDNA synthesis kit	Bio-Rad	1708891
Biotin RNA Labeling Mix	Sigma-Aldrich	11685597910
TruSeq mRNA library preparation kit	illumina	20020595
Deposited data		
Raw and analyzed data	This paper	GEO: GSE167075
Experimental models: Cell lines		
Caco-2 cells	ATCC	HTB-37
Calu-3 cells	ATCC	HTB-55
Vero E6	ATCC	CRL-1586
Software and algorithms		
Graphpad Prism 8	Software	https://www.graphpad.com/scientific-software/prism/
Bowtie2	Software	http://bowtie-bio.sourceforge.net/bowtie2/index.shtml

(Continued on next page)

Continued

REAGENT or RESOURCE	SOURCE	IDENTIFIER
STAR	Software	https://github.com/alexdobin/STAR
MACS2	Software	https://github.com/macs3-project/MACS
m6A viewer	Software	http://dna2.leeds.ac.uk/m6a/
HTSeq	Software	https://htseq.readthedocs.io/en/master/
DESeq2	Software	https://bioconductor.org/packages/release/bioc/html/DESeq2.html
Cutadapt	Software	https://cutadapt.readthedocs.io/en/stable/

RESOURCE AVAILABILITY

Lead contact
Further information and requests for reagents may be directed to the lead contact, Tariq Rana (trana@ucsd.edu).

Materials availability
Reagents or materials used in this work may be requested from the lead contact by signing a completed material transfer agreement.

Data and code availability
Sequencing data for this study has been submitted to the NCBI Gene Expression Omnibus (GEO; https://www.ncbi.nlm.nih.gov/geo/) and accession number is GEO: GSE167075. Mendeley Data: at http://dx.doi.org/10.17632/6n65z4sv9c.1

EXPERIMENTAL MODEL AND SUBJECT DETAILS

Cell lines and virus strain
All studies were performed based on the approved IRB protocols by the University of California (UCSD), San Diego. The human colorectal adenocarcinoma Caco-2 cells and lung adenocarcinoma Calu-3 cells were purchased from ATCC. 293FT cells were maintained in DMEM medium with 10% FBS. Caco-2 and Calu-3 cells were cultured in high-glucose MEM (Thermo Fisher Scientific) supplemented with 20% fetal bovine serum (FBS; GIBCO), MEM NEAA (Thermo Fisher Scientific) and 50 U/ml penicillin-streptomycin (GIBCO) in a humidified 5% CO_2 atmosphere.

For SARS-CoV-2 live cell infection, SARS-CoV-2 isolate USA-WA1/2020 was obtained from BEI Resources. SARS-CoV-2 virus was propagated, and infectious units were quantified by plaque assay using Vero E6 cells.

METHOD DETAILS

Generation of knockdown cell lines
Control, METTL3 or METTL14 depletion cell lines were generated using lentiviral shRNA system. shRNAs targeting METTL3 or METTL14 were described previously (Lichinchi et al., 2016a, 2016b). Lentiviruses were generated by co-transfecting HEK293T cells with the shRNA expressing PLKO vectors (carrying a puromycin resistance gene), a packaging plasmid (psPAX2), and an envelope plasmid (pMD2.G) in DMEM medium. At 14 h after transfection, the medium was replaced with DMEM/10% FBS. After two days of transfection, the supernatants were collected and used to infect Caco-2 or Calu-3 cells by spin infection. Transduced cells were selected by culture with puromycin (Alfa Aesar) at 2 μg/ml (Caco-2) or 4 μg/ml (Calu-3) for at least 7 days, and knockdown efficiency was determined by RT-qPCR or western blot analysis.

SARS-CoV-2 viral infection, SARS-CoV-2-N IVT RNA production, transfection, and inhibitor treatment
Stable Caco-2 or Calu-3 cells transduced with shControl, shMETTL3 or shMETTL14 were infected with SARS-CoV-2 at MOI = 2 for 1h at 37°C. Then cells were washed, and fresh culture medium was supplemented. 24 hours post-infection, infected cells or supernatant were lysed using TRIzol /TRIzol LS and RNA was extracted using a Direct-zol RNA Kit (Zymo). When treated with IκBα phosphorylation inhibitor, cells were pretreated with IκBα phosphorylation inhibitor Bay 11-7085 (R&D Systems) at concentrations of 10 μM for 1 hour at 37°C before infection.

For IVT-SARS-CoV-2-N experiments, N gene was amplified from pcDNA3.1(+)-N-eGFP-N plasmid (GenScript) by PCR primer: Cov-T7-N-F (tactgTAATACGACTCACTATAGGatgtctgataatggaccccaaaatc;) and polyT-N-R ((t)37aggcctgagttgagtcagcac). Purified PCR products were used as a template for IVT by mMESSAGE mMACHINE T7 Transcription Kit (capped RNA; Thermo Fisher) or MEGAscript T7 Transcription Kit (uncapped RNA, Thermo Fisher). The IVT RNAs were purified by MEGAclear Transcription Clean-Up Kit (Thermo Fisher). IVT RNAs were transfected to indicated control and knockdown cells at same amount by Lipofectamine 3000 according to the company instructions (Thermo Fisher). RNAs were extracted 12-16 hours after IVT transfection.

When treated with IκBα phosphorylation inhibitor, cells transfected with IVT RNA, and pretreated with IκBα phosphorylation inhibitor Bay 11-7085 (R&D Systems) at concentrations of 10 μM for 1 hour at 37°C before collecting cells.

MeRIP-seq and MeRIP-RT qPCR of SARS-CoV-2 virus

MeRIP-Seq and MeRIP-qPCR was performed as previously reported (Li et al., 2020; Lichinchi et al., 2016b). Briefly, supernatant or cellular RNAs were purified from viral infected-Vero or Caco-2 cells. The RNAs were treated with DNaseI, concentrated and quantified. Purified RNA was fragmented to 100–200 nucleotides using Ambion RNA Fragmentation Reagent (AM8740, Life Technologies) and the fragmented RNA purified by ethanol precipitation. An input sample (10% of total fragmented RNA) was reserved. Fragmented RNA was incubated with 10 μL rabbit anti-m6A polyclonal Ab (ab151230, Abcam) in IP binding buffer (10 mM Tris-HCl, 150 mM NaCl, 0.1% NP-40, pH 7.4) for 2 h at 4°C. The mixture was then incubated with 50 μL protein A/G magnetic beads (Thermo Fisher) for 2 h at 4°C, and the beads were collected and washed twice in IP wash buffer (10 mM Tris-HCl, 1 M NaCl, 0.1% NP-40, pH 7.4). Bound RNA was eluted from the beads with m6A elution buffer (10 mM Tris-HCl, 1 M NaCl, 0.1% NP-40, 25 mM m6A, pH 7.4) and extracted with RNA Clean & Concentrator Kits (ZYMO). Input and m6A-containing viral RNA were dissolved in water and either reverse transcribed by iScript cDNA synthesis kit (Bio-Rad) and analyzed by qPCR or processed for library generation using a TruSeq mRNA library preparation kit (Illumina). Sequencing was performed by Illumina NovaSeq 6000 at the IGM Genomics core, UCSD.

MeRIP-seq data analysis

Sequencing reads were aligned to SARS-CoV-2 or human genome by Bowtie2 or STAR. Then m6A peaks were called by m6A viewer or MACS2 based on its paired m6A-RIP/input data from the aligned reads: m6A viewer (expected peak length 200, enrichment fold > 3, FDR < 0.01, Minimum Peak Height:10000) and MACS2 (p value < 0.05, call-summit, no model, BAMPE, maximum duplicate fragments = 1 or keep all duplicates for SARS-CoV-2, and keep-dup auto, extsize 200, nomodel, p value < 1e-5 for human). The peak region and summit of each alignment and peak calling strategy were summarized in Tables S1 and S2.

RNA-seq and data analysis

For RNA-Seq, total RNAs were extracted from SARS-CoV-2-infected shControl and shMETTL3 Caco-2 cells (three biological replicates). Sequencing was performed by Illumina NovaSeq 6000 at the IGM Genomics Center, UCSD. Fastqc was used to perform quality control on sequencing data, and Cutadapt was used to remove adapters and trim reads. The preprocessed reads were then aligned to the human or SARS-CoV-2 genome using STAR. The raw gene count for each sample was obtained by htseq-count and the differential gene expression analysis was performed by DEseq2.

RT-qPCR

Total RNA was extracted from SARS-CoV-2 infected or IVT-CoV2 transfected cells by Quick-RNA Miniprep Plus Kit (Zymo Research) according to the manufacturer's instructions. All RNAs were treated with DNase I. cDNAs were synthesized using an iScript cDNA synthesis kit (Bio-Rad). Gene expression levels were normalized to glyceraldehyde 3-phosphate dehydrogenase (GAPDH) or 18S RNA levels and are expressed as the relative fold-change in expression compared with the control condition.

Western blot analysis

Cells were lysed in lysis buffer (60 mM Tris HCl, 2% SDS, 10% glycerol, complete EDTA-free protease inhibitor, 500 U/ml benzonase nuclease) by pipetting. Samples were clarified by centrifugation and protein concentrations in the supernatants were determined with a BCA protein assay kit (Pierce). Aliquots of 30-50 μg of protein were resolved by 4%–12% Bis-Tris Plus PAGE and the proteins were transferred to PVDF membranes. Membranes were blocked with 5% non-fat milk and incubated overnight at 4°C with Abs against RIG-I (20566-1-AP, Proteintech; MABF297, MilliporeSigma), IRF-3 (D614C, Cell Signaling Technology), IκBα (L35A5, Cell Signaling Technology), Phospho-IRF-3 (Ser386) (E7J8G, Cell Signaling Technology), Phospho-IκBα (Ser32/36) (5A5, Cell Signaling Technology), METTL3 (15073-1-AP, Proteintech) or GAPDH (14C10, Cell Signaling Technology). After washing, the membranes were incubated for 1 h at RT with secondary Ab. Finally, the blots were developed using ECL and imaged.

RNA immunoprecipitation (RIP)

RIP assays were carried out based on previous published method (Peritz et al., 2006). Briefly, for live viral binding experiments, equal copy number of SARS-CoV-2 virus from infected Caco-2 cells or METTL3 knockdown cells were incubated with equal amount of immunoprecipitated RIG-I proteins for 2hrs at room temperature. RIG-I bound viral RNAs were washed by lysis buffer and purified as described below. For IVT-RNA experiments, control or METTL3 knockdown Caco-2 cells were transfected with equal amount of wild-type or m6A mutant IVT-CoV2 RNAs, cells were collected for RIP experiments 16 hours post transfection. Ten million cells were used for one IP. Cells were lysed in 2 mL of polysome lysis buffer (100 mM KCl, 5 mM MgCl₂, 10 mM HEPES, pH 7.0, 0.5% Nonidet P-40, 1 mM DTT, 100 U ml⁻¹ RNasin RNase inhibitor, 2 mM vanadyl ribonucleoside complexes, protease inhibitor cocktail), centrifuged and collected the supernatant. Cell lysates were precleared in protein A/G magnetic beads (Pierce) at 4°C for 1 hour. Save 10% of lysate as whole cell lysis input. Precleared cell lysates were incubated with RIG-I antibody (20566-1-AP, Proteintech) at 4°C overnight. Add 100 μL of protein A/G magnetic beads to each aliquot. Rotate at 4°C for 4 h. Wash the beads with polysome lysis buffer for three times, and then wash the beads with polysome lysis buffer including 1 M urea for three time. Save 10% of beads to check IP

efficiency. Resuspend the remaining beads in 100 μL of polysome lysis buffer with 0.1% SDS and 30 μg proteinase K. Incubate in a heating block at 50°C for 30 min. Add one volume (100 μl) of phenol–chloroform–isoamyl alcohol mixture and vortex to mix. Centrifuge for 1 min to separate phases. Recover (upper) water phase. Repeat the elution step for another time and combine the water phase. Extract RNAs with RNA Clean & Concentrator Kits (ZYMO). The immunoprecipitated RNAs were reverse transcribed by iScript cDNA synthesis kit (Bio-Rad) and analyzed by qPCR.

Biotinylated RNA pulldown assay

RNAs were biotin labeled by in-vitro transcription with Biotin RNA Labeling Mix (Sigma-Aldrich). Biotinylated RNAs were incubated with cell lysates directly or transfected into Caco-2 cells and collect the cell lysates. For transfection experiments, 2.5×10^{14} copies biotinylated RNAs were transfected into Caco-2 cells seeded in a 10-cm dish, transfected cells were lysed in lysis buffer (100 mM KCl, 5 mM MgCl$_2$, 10 mM HEPES, pH 7.0, 0.5% Nonidet P-40, 1 mM DTT, 100 U ml^{-1} RNasin RNase inhibitor, 2 mM vanadyl ribonucleoside complexes, protease inhibitor cocktail), 3.5mg of clarified protein lysates were incubated with 100 μl streptavidin magnetic Beads (NEB) for 1h at room temperature. Beads were washed for four times with lysis buffer and were boiled in SDS-PAGE sample buffer. For direct binding assay, Caco-2 cells were lysed in binding buffer (25 mM Tris-HCl [pH 7.5],150 mM NaCl, 1.5 mM MgCl$_2$, 0.5% Triton X-100, EDTA-free protease inhibitor cocktail). 1×10^{14} copies biotinylated RNAs were incubated with 1mg clarified protein lysate in 150μl binding buffer and incubate by rotating for 30 minutes in room temperature. Then 100 μl streptavidin magnetic Beads (NEB) were added to the mixture and incubated for 1h. Beads were washed for four times with binding buffer and beads were boiled in SDS-PAGE sample buffer. RNA bound RIG-I proteins were analyzed by Western Blot.

LC-MS/MS/MS quantification of SARS-CoV-2 RNA modifications

SARS-CoV-2 genome RNA modifications were analyzed by LC-MS/MS as previously described. SARS-CoV-2 viral RNAs were purified from infected Vero cells. The viral RNA was treated with DNaseI, concentrated and quantified. Purified SARS-CoV-2 viral RNAs were used for the analysis, the data was presented as mean ± SD. Enzymatic digestion was preformed using previously published method (Wang et al., 2014). Briefly, 50 ng of mRNA was incubated at 37°C for 2 hr with 0.5 unit of nuclease P1 in a 25 μL buffer containing 25 mM NaCl and 2.5 mM ZnCl$_2$. To the resulting mixture were subsequently added alkaline phosphatase (0.25 unit) and 3 μL of 1.0 M NH$_4$HCO$_3$ buffer. After incubation at 37°C for an additional 2 hr, the digestion mixture was dried by Speed-vac and reconstituted in 100 μL of ddH2O. Profiling and quantifications of modified ribonucleosides were conducted by employing a nano-flow liquid chromatography-multi-stage mass spectrometry (nLC-nESI-MS/MS/MS) method (Gonzalez et al., 2020). In short, to 10 ng of digested viral RNA were added the following stable isotope-labeled standard nucleosides: 3.3 pmol [^{13}C$_5$]-adenosine, 42.5 fmol D$_3$-N^6-methyladenosine, 17.25 fmol of [^{13}C$_5$]-2′-O-methyladenosine, 9.7 fmol [^{13}C$_5$]-2′-O-methylcytidine, 3.3 pmol [^{15}N$_3$]-cytidine, 5.5 pmol of [^{15}N$_2$]-uridine, 5.1 fmol [^{13}C$_5$]-5-methylcytidine, and 5.6 fmol ^{13}C$_5$-5-methyluridine. The enzymes in the digestion mixture were then removed by chloroform extraction. The aqueous layer was subsequently dried and reconstituted in 100 μL of ddH$_2$O/ acetonitrile (1/9, v/v) to precipitate residual salts in the digestion mixture. After incubation at −20°C for 20 min, the mixture was centrifuged, and the supernatant was collected, dried by Speed-Vac, reconstituted in water, and subjected to LC-MS/MS and MS/MS/MS analyses. nLC-nESI-MS/MS/MS experiments in scheduled in SRM mode were performed on an LTQ-XL linear ion trap mass spectrometer coupled with an EASY-nLC II (Thermo Fisher Scientific, San Jose, CA). The mass spectrometer was operated in the positive-ion mode, with the electrospray, capillary, and tube lens voltages being 2.0 kV, 12 V, and 100 V, respectively. Samples were loaded onto a 5 cm in-house packed porous graphitic carbon (PGC, 5 μm in particle size, Thermo Fisher Scientific) trapping column (150 μm i.d). Analytes were eluted onto a 20-cm Zorbax SB-C18 (5 μm in particle size, 100 Å in pore size, Michrom BioResources) analytical column (75 μm i.d.) at a flow rate of 300 nL/min. The gradient employed was 0%–16% B in 5 min, 16%–22% B in 23 min, 22%–50% B in 17 min, 50%–90% B in 5 min, and finally 30 min at 90% B, using 0.1% (v/v) formic acid in water and 0.1% (v/v) formic acid in acetonitrile as mobile phases A and B, respectively. Isotopically labeled standards were not available for some the modified nucleosides. Hence, we employed stable isotope labeled forms of other nucleosides, which exhibited similar elution times as the modified nucleosides, as surrogate standards for the quantification. The calibration curves for rA, Am, m^{6}A, rC, Cm, and m^{5}C were reported previously (Fu et al., 2015).

QUANTIFICATION AND STATISTICAL ANALYSIS

Data are presented as the mean ± standard error (SEM) unless otherwise indicated. Group means were compared by Student's t test. $p < 0.05$ (*), $p < 0.01$ (**), and $p < 0.001$ (***) indicate statistically significant changes. N represents biological replicates. All the statistical details of experiments can be found in figure legends.